Polyaniline/MWCNTS-$MoSe_2$: A Promising Electrode material for High performance Supercapacitors

By

Bakhtawer Ejaz

School of Chemical and Materials Engineering

National University of Sciences and Technology

July 2023

Polyaniline/MWCNTS-$MoSe_2$: A Promising Electrode material for High performance Supercapacitors

Bakhtawer Ejaz
Reg.No:00000320586

This thesis is submitted as a partial fulfillment of the requirements for the degree of

"Master of Science (MS) in Nanoscience and Engineering"

Supervisor Name: Dr. Zakir Hussain

School of Chemical and Materials Engineering (SCME)
National University of Sciences and Technology (NUST)
H-12 Islamabad, Pakistan

July 2023

THESIS ACCEPTANCE CERTIFICATE

Certified that final copy of MS thesis written by Ms **Bakhtawer Ejaz** (Registration No 00000320586), of School of Chemical & Materials Engineering (SCME) has been vetted by undersigned, found complete in all respects as per NUST Statues/Regulations, is free of plagiarism, errors, and mistakes and is accepted as partial fulfillment for award of MS degree. It is further certified that necessary amendments as pointed out by GEC members of the scholar have also been incorporated in the said thesis.

Signature: _____

Name of Supervisor: **Dr Zakir Hussain**

Date: 27/9/2023

For Signature (HOD): _____

Date: 27-9-23

Signature (Dean/Principal): _____

Date: 27-9-2023

NSE-07-2019

Form TH-1
(Must be type written)

National University of Sciences & Technology (NUST)

MASTER'S THESIS WORK

Formulation of Guidance and Examination Committee (GEC)

Name: Bakhtawer Ejaz NUST Reg No: 00000320586

Department: Materials Engineering

Specialization: MS Nanosciences and Engineering

Credit Hour Completed: 18 CGPA: 3.23

Course Work Completed

S/No	Code	Title	Core/Elective	CH	Grade
1	MSE-854	Characterization of materials	Core	3	B+
2	NSE-813	Essentials of Nanosciences and Engineering	Core	3	B+
3	MSE-856	Nanomaterials and Processing	Core	3	B+
4	NSE-845	Nanolithography and device fabrication	Elective	3	B
5	MSE-872	Composite Materials	Elective	3	B
6	NSE-812	Environmental Nanotechnology	Elective	3	B
7	RM-898	Research Methodology		3	Q

Date _____ Student's Signature _____

Thesis Committee

1. Name: Dr. Zakir Hussain (Supervisor) Signature: 12/2/202
   Department: Materials Engineering
2. Name: Dr. Aftab Akram Signature: 12/2/2021
   Department: Materials Engineering
3. Name: Dr. I.H Gul Signature:
   Department: Materials Engineering
4. Co supervisor _____ Signature: _____
   Department: _____

Date: 15/2/2021 Signature of Head of Department: _____

APPROVAL

Date: 16.2.2021

Dean/Principal

Distribution

1x copy to Exam Branch, Main Office NUST
1x copy to PGP Dte, Main Office NUST
1x copy to Exam branch, respective institute

National University of Sciences &Technology (NUST)

FORM TH-4

MASTER'S THESIS WORK

We hereby recommend that the dissertation prepared under our supervision by

Regn No & Name: **0000320586 Bakhtawer Ejaz**

Title: **Polyaniline/MWCNTS-$MoSe_2$: A Promising Electrode material for High performance Supercapacitors.**

Presented on: **31 Aug 2023** at: **1500 hrs in SCME Seminar Hall**

Be accepted in partial fulfillment of the requirements for the award of Masters of Science degree in **Nanoscience & Engineering.**

Guidance & Examination Committee Members

Name: **Dr Iftikhar Hussain Gul** Signature:

Name: **Dr M. Aftab Akram** Signature:

Supervisor's Name: **Dr Zakir Hussain** Signature:

Dated: 31/8/2023

Head of Department
Date 31/8/23

Dean/Principal
Date 1.9.2023

School of Chemical &Materials Engineering (SCME)

Dedication

This thesis is dedicated to my parents and husband for their love, support, sacrifices, prayers, and advice.

Acknowledgments

Primarily, praises and thanks to ALLAH Almighty for the blessings he bestowed upon me, gave me strength, good health, and the ability to learn and understand to complete this research successfully. It is a genuine to express my deep and sincere gratitude to my honorable supervisor Prof. Dr Zakir Hussain, the best mentor, for sharing his experience and wealth of knowledge through his kind supervision, valuable guidance, and timely and constructive advice which helped me extensively in accomplishing my research work. Besides my supervisor, I thank profusely my Guidance and Examination Committee (GEC) members Dr. Muhammad Iftikhar Hussain Gul and Dr. Muhammad Aftab Akram, and my fellow lab mates for the guidance, timely suggestions, and effective working environment. I owe a deep sense of appreciation to the lab technicians/engineers for the characterization of samples and assistance in understanding the instrumentations. I also acknowledge the help provided by fellows from the other labs. In addition, I would like to extend my sincere thanks to my best friends for their ceaseless cooperation and support both in and outside the lab throughout my research. I would like to convey my wholehearted gratitude to all the teachers/lecturers I learned from since childhood and everyone who has directly or indirectly helped me throughout my academic journey. Last but not least, huge thanks to my parents and siblings for their unparalleled love, care, encouragement, financial and emotional support, and lots of prayers.

Bakhtawer Ejaz

Abstract

This thesis endeavors to explore the potential of hybrid materials consisting of $MoSe_2$/MWCNTS@PANI as electrode materials for supercapacitors. The primary focus lies in assessing their electrochemical performance, stability, and energy storage capabilities. By investigating synthesis methods, characterizing structural and morphological properties, and conducting extensive electrochemical analyses, this research aspires to provide a comprehensive understanding of the unique advantages and limitations associated with $MoSe_2$/MWCNTS@PANI composites. The outcomes of this study are poised to make meaningful contributions to the advancement of electrode materials for high-performance supercapacitors. Furthermore, they offer valuable insights into the practical applications of these materials in energy storage systems, addressing the critical need for efficient and sustainable energy storage technologies.

To synthesize the PANI-MWCNTs/$MoSe_2$ composite for electrochemical energy storage applications, a straightforward one-pot method was employed. This composite, composed of multiple $MoSe_2$ nanospheres, PANI, and functionalized MWCNTs, exhibits remarkable properties when used as an electrode material in supercapacitors. Specifically, it demonstrates a high specific capacitance of 441 F/g at a scan rate of 20 Vs- and exceptional cycling stability, retaining 90% of its initial capacitance after 10,000 cycles. Notably, these samples showcase the ability to function effectively within a wide potential window (ΔV=2V) when immersed in a 3M KOH solution, rendering them highly suitable candidates for integration into various electronic devices. This outstanding performance is largely attributed to the unique morphology of the composite, which significantly enhances its charge storage capacity. Collectively, these results underscore the potential of PANI@MWCNTs/$MoSe_2$ as promising electrode materials for energy storage devices.

Table of Contents

List of Figures

List of Tables

Chapter 1

Introduction

In recent years, the quest for efficient and sustainable energy storage systems has become increasingly crucial. As the demand for clean energy sources grows and the need for portable electronic devices and electric vehicles expands, there is a pressing need for high-performance energy storage technologies [1]. Supercapacitors, also known as ultracapacitors or electrochemical capacitors, have emerged as a promising solution due to their rapid charge- discharge capabilities, long cycle life, and high-power density.

Supercapacitors are energy storage devices that bridge the gap between conventional capacitors and batteries. They offer high power density, rapid charge-discharge capabilities, and long cycle life. Unlike batteries, which store energy through chemical reactions, supercapacitors store energy through electrostatic charges at the electrode-electrolyte interface. Supercapacitors consist of two electrodes separated by an electrolyte, and their performance relies on the unique properties of the electrode materials [2]. These materials, often carbon-based or transition metal oxides, provide a large surface area for charge storage and efficient ion transport. The major advantages of supercapacitors include their ability to deliver high power bursts, tolerate many charge-discharge cycles, and operate effectively over a wide temperature range. They find applications in various fields such as transportation (electric vehicles), renewable energy systems, consumer electronics, and power backup systems. Researchers continue to explore new electrode materials, electrolytes, and device architectures to enhance the energy density and overall performance of supercapacitors. Their potential to complement or even replace batteries in certain applications makes them a promising technology for addressing energy storage challenges in the future.[3]

Table 1: Comparison of Energy Storage Devices

Characteristic	Capacitor	Supercapacitor	Battery
Specific Energy (W h kg^{-1})	<0.1	1 - 10	10 - 100
Specific power (W Kg^{-1})	>10,000	500 – 10,000	<10,000
Discharge time	10^{-6} to 10^{-3}	s to min	0.3 – 3hr
Charge time	10^{-6} to 10^{-3}	s to min	1 – 5hr
Coulombic efficiency (%)	About 100	85 - 98	70 - 85
Cycle-life	Almost Infinite	>500,000	About 1000

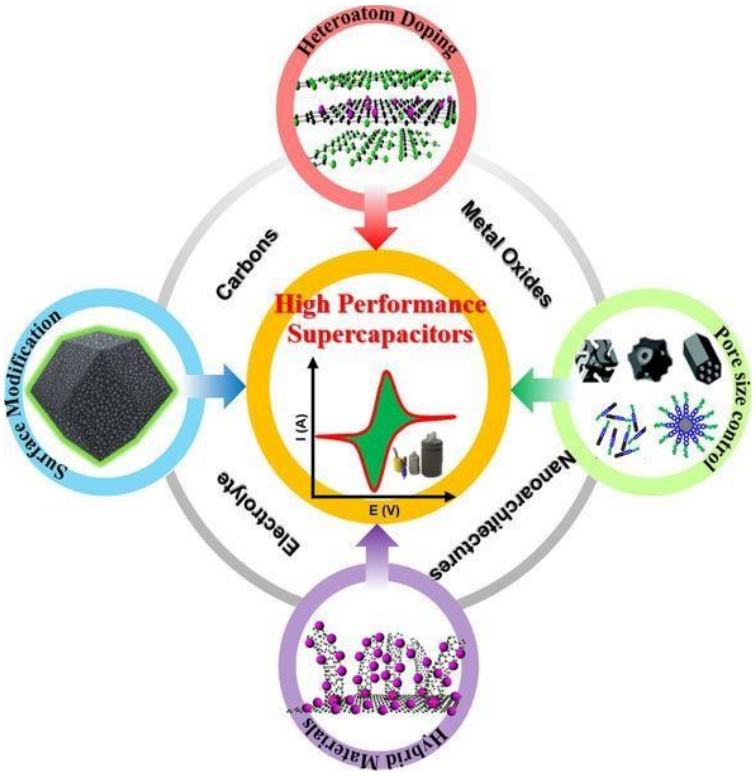

Figure 1 Application of Supercapacitors(Gong et al., 2017)

1.1. Classification of Supercapacitors:

The development of advanced electrode materials is critical for advancing the performance of supercapacitors. $MoSe_2$, CNTS, and PANI have emerged as promising candidates due to their unique properties and synergistic effects [4]. $MoSe_2$ offers high electrical conductivity and abundant active sites, while CNTS provides a conductive framework and prevents aggregation. PANI, as a conducting polymer, introduces pseudocapacitive behavior and enhances charge storage capacity [5]. The combination of these materials in composite structures presents an opportunity to develop high-performance electrode materials for supercapacitors, paving the way for efficient and sustainable energy storage systems [6]. Further research and development in this area hold great promise for realizing the full potential of $MoSe_2$, CNTS, and PANI in advanced energy storage applications.[7]

Supercapacitors are classified primarily based on the type of electrodes employed, as their performance is influenced by this aspect. As depicted in figure 2, there are three main categories of SCs: hybrid supercapacitors, pseudo capacitors, and electrical double-layer capacitors (EDLCs).[8]

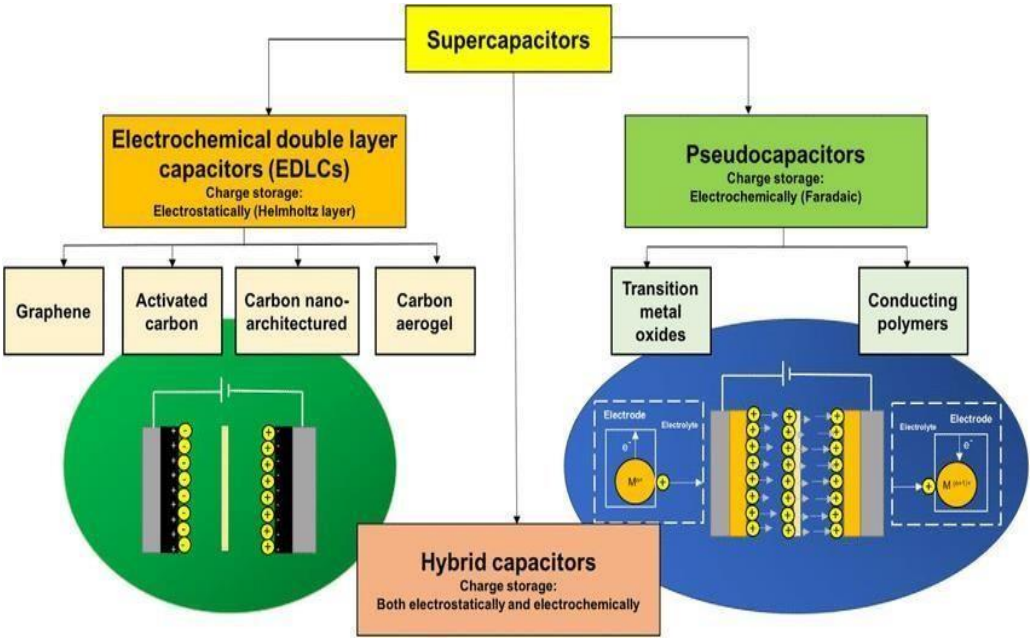

Figure 2 Classification of Supercapacitors

1.2. Electrochemical double layer Capacitors (EDLCs)

EDLCs (Electric Double-Layer Capacitors), also known as supercapacitors, consist of three main components. The first component comprises two electrodes composed primarily of carbon materials, with carbon nanotubes and graphene being commonly used. The second component is the separator, while the third component is the electrolyte. In EDLCs, the transfer of charge between the electrolyte and electrode material does not occur through a faradic process. Instead, it is stored electrostatically on the surface of the electrode.

material [9]. This phenomenon leads to the formation of double layers at the surface of the electrodes, where energy is stored electrochemically. When a voltage is applied to the EDLCs, ions move from the electrolyte through the separator and migrate toward the electrode with the opposite charge. The voltage supply creates an attractive force between opposite charges, causing the accumulation of charges on the surface of the electrodes.[10]

In addition to the advantages mentioned earlier, the storage system used by EDLCs offers improved power performance and rapid energy uptake and delivery. This is due to the absence of any chemical reactions resulting from the non-faradic process [10]. Unlike batteries, EDLCs do not experience active material swelling during charging and discharging, making them more

durable and capable of withstanding a high number of charge-discharge cycles (>105 cycles). The capacitance resulting from the development of the double layer typically [11] ranges from 5 to 20 μF cm 2, depending on the type of electrolyte utilized. Notably, using acidic or aqueous alkaline electrolytes in EDLCs yields significantly higher specific [12] capacitances compared to organic electrolytes. However, one drawback of EDLCs is that the voltage window they can operate within is relatively small, leading to a lower energy density.

$$E = \frac{1}{2} CV^2$$

The energy density in capacitors is influenced by several factors, including:

- Capacitance: Higher capacitance values result in increased energy storage capacity.
- Voltage Window: A wider voltage window allows for more energy storage.
- Operating Temperature: Different temperature ranges can affect the performance of EDLCs.
- Electrode Materials: Researchers are actively working on developing new materials to enhance the energy density of EDLCs.
- Electrolytes: The choice of electrolyte can impact the overall energy storage capabilities.

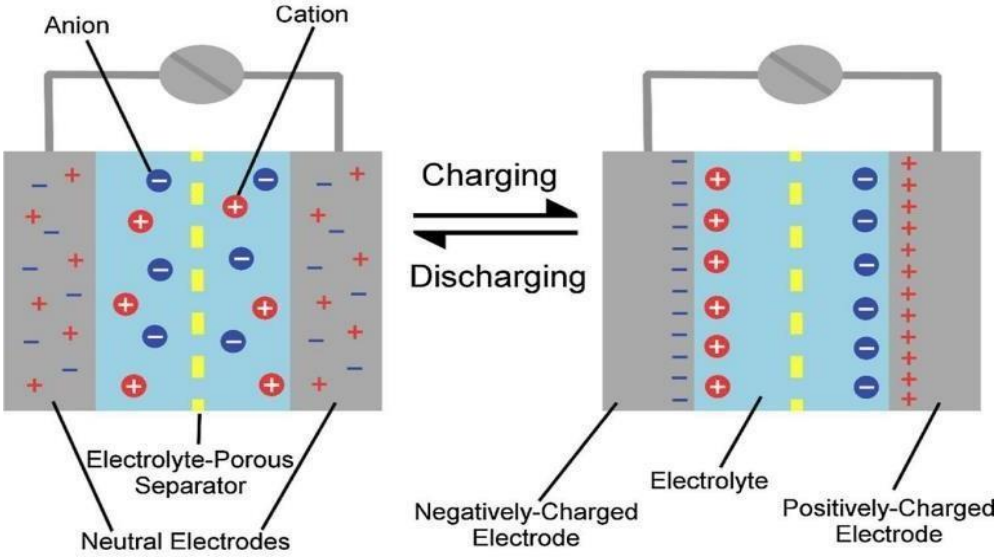

Figure 3 Charge Storage Mechanism of EDLC(Akib Hasan, Sayantha Aniv, & Mominul Islam, 2023)

Due to their relatively low energy density, EDLCs may not be suitable for applications requiring high energy storage. However, ongoing research and advancements in materials, electrolytes, and design may lead to improvements in EDLCs' energy density and expand their potential applications in the future. [13]

Chapter 2

Literature Review

In the past few years, there has been a growing focus among researchers on supercapacitors. Recent progress in electrode materials and technological innovations has led to a reduction in the distinction between capacitors and batteries, bridged by the emergence of supercapacitors. Figure 10 illustrates the materials employed in recent times, along with the quantity of research endeavors dedicated to supercapacitors over the preceding two decades.[20]

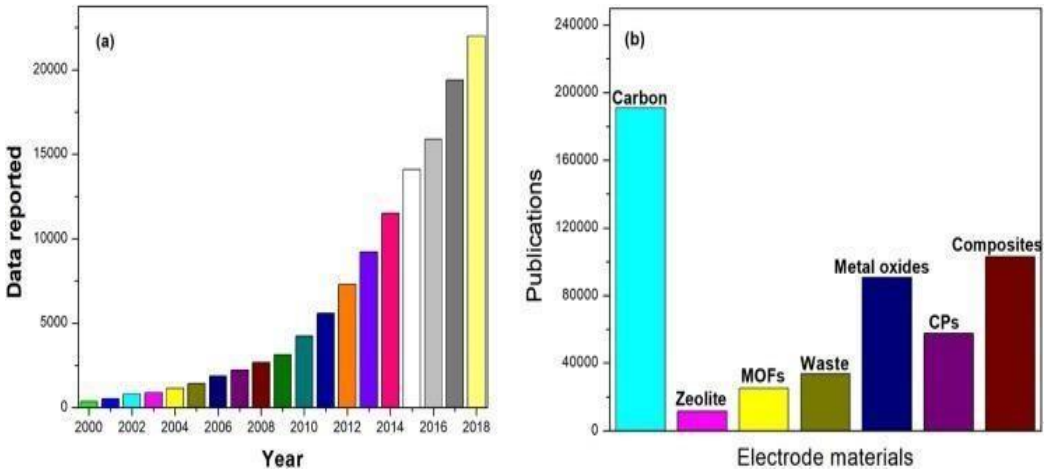

Figure 4 (a) Research publications (b) publications on electrode material (Innocenzi & Malfatti, 2013)

2.1. Nanomaterials:

2.1.1. Introduction

Nanomaterials are materials that possess unique properties and characteristics at the nanoscale, typically ranging from 1 to 100 nanometers in size. These materials exhibit distinct physical,

chemical, mechanical, and optical properties compared to their bulk counterparts [22]. The emergence of nanotechnology has enabled the synthesis, manipulation, and application of nanomaterials, leading to advancements in various fields, including electronics, medicine, energy, and materials science.[23]

One of the defining features of nanomaterials is their high surface-to-volume ratio. With a large surface area, nanomaterials offer increased opportunities for interactions with other materials or environments, making them highly versatile and suitable for numerous applications [12]

Diverse types of nanomaterials have been developed, each with its unique properties and synthesis methods.[24]

One prominent category of nanomaterials is nanoparticles. These are particles with dimensions on the nanoscale, often spherical or rod-shaped. Nanoparticles can be synthesized using different techniques such as chemical methods, physical vapor deposition, or biological approaches(Akib Hasan et al., 2023). They can be composed of metals, metal oxides, semiconductors, or polymers. Due to their small size, nanoparticles exhibit enhanced optical, electronic, and catalytic properties, making them useful in fields such as electronics, sensors, catalysis, and drug delivery systems.[25]

Figure 5 Schematic representation of nanomaterials and their applications

2.2. Selenium based Nanoparticles.

Selenium-based nanoparticles have gained significant attention due to their unique properties and potential applications in various fields, including medicine, electronics, energy, and environmental remediation. Selenium (Se) is a non-metal element with different allotropes, and nanoparticles based on selenium can be synthesized using various methods.

Selenium nanoparticles exhibit size-dependent properties, and their size, shape, and surface characteristics can be tailored to achieve specific functionalities. These nanoparticles possess excellent optical, electrical, and catalytic properties, making them versatile for a wide range of applications.[28]

In the field of medicine, selenium-based nanoparticles have shown promise for drug delivery systems, imaging agents, and therapeutics. Their biocompatibility and low toxicity make them suitable for biomedical applications. Selenium nanoparticles can be functionalized with specific targeting ligands to deliver drugs or imaging agents to targeted cells or tissues, enhancing their efficacy, and reducing side effects.[29]

In the electronics industry, selenium nanoparticles have been investigated for their potential use in optoelectronic devices, photovoltaics, and sensors. The unique optical properties of selenium nanoparticles, such as tunable photoluminescence and quantum confinement effects, make them attractive for applications in LEDs, solar cells, and sensors for detecting gases or biomolecules.

Selenium nanoparticles also exhibit excellent catalytic properties, enabling their use as catalysts in various chemical reactions. They have been employed as catalysts for organic transformations, environmental remediation, and fuel cells. Selenium nanoparticles can provide high catalytic activity, selectivity, and stability, making them valuable for sustainable and efficient chemical processes.[29]

Furthermore, selenium-based nanoparticles have shown promise in environmental applications, particularly in the removal of heavy metals and pollutants from water. Selenium nanoparticles can be functionalized to selectively bind with specific contaminants, facilitating their removal from contaminated water sources. Their high surface area and reactivity make those efficient adsorbents for pollutants, offering potential solutions for water purification and environmental remediation.[30]

It is worth noting that the synthesis and characterization of selenium nanoparticles require careful consideration of factors such as reaction conditions, stabilization methods, and surface modifications. Various synthesis techniques, including chemical reduction, solvothermal methods, and biological approaches, have been employed to produce selenium nanoparticles with controlled size, shape, and surface properties.

In conclusion, selenium-based nanoparticles hold immense potential in diverse fields due to their unique properties. Their applications range from medicine and electronics to catalysis and environmental remediation. Continued research and development in the synthesis, functionalization, and characterization of selenium nanoparticles will further expand their applications and contribute to advancements in nanotechnology.[31]

These are just a few examples of the types of nanoparticles available. The field of nanotechnology continues to advance, leading to the development of novel nanoparticles and their applications across various industries.

2.2.1. Molybdenum Di selenide

Molybdenum Di selenide ($MoSe_2$) is a two-dimensional (2D) transition metal dichalcogenide (TMD) material that has gained significant attention in recent years. It belongs to the family of layered materials, which includes other popular TMDs such as molybdenum disulfide (MoS_2) and tungsten Di selenide (WSe_2). $MoSe_2$ consists of a hexagonal lattice of molybdenum atoms sandwiched between two layers of selenium atoms.

$MoSe_2$ (Molybdenum Di selenide) has garnered significant attention as a promising material for energy storage applications. It is a two-dimensional (2D) transition metal dichalcogenide (TMD) that belongs to the same family as graphene. $MoSe_2$ possesses unique properties that make it an attractive candidate for electrode materials in supercapacitors. Firstly, it exhibits high electrical conductivity, enabling efficient electron transfer within the electrode material. This property is essential for achieving fast charge-discharge rates and high-power density, which are key requirements for supercapacitor applications. Additionally, $MoSe_2$ has a layered structure with abundant active sites, providing ample opportunities for charge storage and ion adsorption. These characteristics contribute to enhanced capacitance and improved energy storage capabilities.

$MoSe_2$ exhibits intriguing properties due to its unique atomic structure and reduced dimensionality. In its bulk form, $MoSe_2$ is an indirect bandgap semiconductor, but when thinned down to monolayer

or few-layer thicknesses, it becomes a direct bandgap semiconductor with remarkable optical and electronic properties. This makes $MoSe_2$ a promising candidate for various electronic and optoelectronic applications.

One of the notable characteristics of $MoSe_2$ is its strong interaction with light. It has a direct bandgap in the visible to near-infrared range, enabling efficient light absorption and emission. This property makes $MoSe_2$ attractive for applications in photodetectors, solar cells, and light- emitting diodes (LEDs). Additionally, $MoSe_2$ has been studied for its potential in valleytronics, a field that utilizes the valley degree of freedom in materials to encode and process information.

$MoSe_2$ also exhibits excellent electrical properties. It has high electron mobility, making it suitable for use in field-effect transistors (FETs) and other electronic devices. $MoSe_2$-based FETs have shown reliable performance, with high on/off current ratios and low power consumption. The 2D nature of $MoSe_2$ allows for atomically thin devices, enabling the miniaturization of electronic components.

Furthermore, $MoSe_2$ demonstrates intriguing mechanical properties. It has high flexibility and can withstand large mechanical deformations without breaking. This property has led to the exploration of $MoSe_2$ in flexible electronics and strain sensors.

In addition to its electrical and optical properties, $MoSe_2$ also exhibits strong catalytic activity. It can function as an efficient catalyst for various chemical reactions, including hydrogen evolution reaction (HER), oxygen reduction reaction (ORR), and water splitting. These properties make $MoSe_2$ a potential candidate for energy conversion and storage applications, such as fuel cells and electrochemical supercapacitors.

The synthesis of $MoSe_2$ can be achieved through different methods, including chemical vapor deposition (CVD), mechanical exfoliation, and solution-based approaches. CVD allows for the controlled growth of large-area $MoSe_2$ films, while mechanical exfoliation enables the production of high-quality $MoSe_2$ monolayers. Solution-based methods provide a scalable approach for producing $MoSe_2$ nanoparticles or thin films.[31]

In conclusion, $MoSe_2$ is a fascinating 2D material with diverse properties and potential applications. Its unique optical, electrical, mechanical, and catalytic properties have attracted considerable interest in fields ranging from electronics and optoelectronics to energy conversion

and storage. Ongoing research continues to explore the full potential of MoSe2 and its integration into various technological devices and systems.

2.3. Carbon nano Tubes

Carbon exhibits sp2 hybridization in its elemental form, giving rise to various structures such as graphite and other remarkable formations. Carbon nanotubes (CNTs) are fascinating nanostructures that have captivated the attention of researchers and scientists due to their unique properties and potential applications in various fields. CNTs are cylindrical structures made up of carbon atoms arranged in a hexagonal lattice [32], forming seamless tubes with diameters on the nanometer scale. These structures can be considered as rolled-up sheets of graphene, resulting in exceptional mechanical, electrical, and thermal properties. There are two main types of carbon nanotubes: single-walled carbon nanotubes (SWCNTs) and multi-walled carbon nanotubes (MWCNTs) [33]. SWCNTs consist of a single layer of graphene rolled into a seamless cylinder, resembling a hollow tube. They possess remarkable properties such as high tensile strength, exceptional electrical conductivity, and unique optical properties. The diameter of SWCNTs typically ranges from about 0.4 to 2 nanometers.[34]

CNTS (Carbon Nanotubes) have long been recognized for their exceptional electrical, mechanical, and thermal properties. These hollow cylindrical structures, composed of rolled- up graphene sheets, offer a high aspect ratio and a large surface area, making them an ideal candidate for electrode materials in supercapacitors. The presence of CNTS in composite materials can significantly enhance the overall electrochemical performance [34]. CNTS provides a highly conductive framework throughout the electrode material, facilitating the rapid transport of electrons and ions [35]. This, in turn, leads to improved charge-discharge rates and enhanced energy storage capacity. Furthermore, the interconnected network of CNTS prevents the aggregation of active materials, ensuring efficient utilization and promoting cycling stability.[36]

On the other hand, MWCNTs consist of multiple layers of graphene stacked concentrically, forming a tube within a tube structure. These tubes can be thought of as a series of nested cylinders. MWCNTs exhibit excellent mechanical strength and offer enhanced structural stability compared to SWCNTs. The diameter of MWCNTs varies, typically ranging from 1 to 3 nanometers. Both SWCNTs and MWCNTs have garnered significant attention in various fields of research and technological applications. Their exceptional properties make them promising candidates for a

wide range of applications, including electronics, energy storage, aerospace, biomedicine, and environmental remediation. Researchers are continually exploring and harnessing the unique properties of carbon nanotubes to unlock their full potential and revolutionize various industries. There are several methods for producing carbon nanotubes (CNTs), each with its own advantages and limitations.[37]

Here are some commonly used methods:

Arc Discharge: In this method, a high-current electric arc is generated between two graphite electrodes in an inert gas atmosphere. The high temperature and pressure conditions cause carbon atoms to vaporize and condense into nanotubes.

Laser Ablation: In this technique, a laser beam is focused on a graphite target inside a high-temperature furnace. The intense heat generated causes the graphite to evaporate, and the carbon vapor condenses into nanotubes on a cooler substrate.

Chemical Vapor Deposition (CVD): CVD is a widely used method for synthesizing CNTs. It involves the decomposition of carbon-containing precursor gases, such as hydrocarbons, in the presence of a catalyst at elevated temperatures. The carbon atoms then deposit onto a substrate, forming nanotubes.

Catalytic Chemical Vapor Deposition (CCVD): CCVD is a variation of CVD that involves the use of metal catalysts, such as iron, nickel, or cobalt, to promote the growth of nanotubes. The catalyst particles function as nucleation sites for carbon deposition, leading to the formation of CNTs.

High-Pressure Carbon Monoxide (HiPCO) Process: In this method, carbon monoxide gas is decomposed at high pressures and temperatures in the presence of iron-based catalyst particles. The resulting carbon atoms form nanotubes.

Electric Arc Discharge in Liquid: Similar to the arc discharge method, this technique involves the application of a high electric current between two electrodes submerged in a liquid medium. The liquid acts as a template, allowing the growth of CNTs with controlled characteristics.

Template-based Synthesis: This method utilizes porous templates, such as alumina or silica, with nanoscale pores. Carbon precursors are then deposited onto the template, and after subsequent

treatments, the template is removed, leaving behind aligned CNTs.

These are just a few examples of the methods used to produce carbon nanotubes. Each method has its own advantages, such as scalability, control over nanotube properties, and cost effectiveness. The choice of method depends on the desired properties of the nanotubes and the specific application requirements. Ongoing research continues to explore new techniques and optimize existing methods for the synthesis of CNTs with improved quality and scalability.

2.3.1. Functionalization of CNTS

Functionalization of carbon nanotubes (CNTs) involves modifying their surface properties by attaching various functional groups or molecules. This process enhances the dispersibility, compatibility, and reactivity of CNTs, thereby expanding their potential applications. Functionalized CNTs offer improved interactions with other materials, enabling tailored properties and functionalities. Here are some common types of functionalization for CNTs:

Covalent Functionalization: In this approach, functional groups are covalently bonded to the carbon nanotube surface. Chemical reactions, such as diazonium chemistry, Friedel-Crafts reactions, or radical addition reactions, are employed to attach functional groups. Covalent functionalization provides strong and durable bonds but may alter the electronic structure of CNTs. Covalent functionalization involves the formation of strong and durable chemical bonds between functional groups and the carbon nanotube surface. This approach modifies the electronic structure of CNTs and can significantly alter their properties. Covalent functionalization is achieved through various chemical reactions, such as diazonium chemistry, Friedel-Crafts reactions, or radical addition reactions. These reactions create stable linkages between the functional groups and the CNT surface. Covalent functionalization provides several advantages. Firstly, it offers precise control over the type and density of functional groups attached to CNTs. This enables tailored surface properties and targeted interactions with other materials. Secondly, covalent functionalization enhances the dispersibility of CNTs in solvents and matrices, promoting their homogeneous integration into various systems. Additionally, covalently functionalized CNTs exhibit improved chemical stability and resistance to degradation, making them suitable for applications in harsh environments.

Non-Covalent Functionalization: Unlike covalent functionalization, non-covalent

functionalization involves weak interactions, such as π-π stacking, van der Waals forces, or hydrogen bonding, between the CNT surface and functional molecules. This method preserves the intrinsic properties of CNTs and allows reversible functionalization. Non-covalent functionalization involves the weak interactions between the CNT surface and functional molecules without forming strong chemical bonds. This approach preserves the inherent properties of CNTs while imparting additional functionalities through physical adsorption or supramolecular interactions. The non-covalent functionalization methods commonly used with CNTs include π-π stacking, van der Waals forces, hydrogen bonding, and electrostatic interactions. Non-covalent functionalization offers several advantages. It allows for reversible attachment and detachment of functional molecules, enabling dynamic interactions and facile modification of CNTs' properties. This method maintains the electronic structure of CNTs, ensuring their intrinsic electrical and thermal conductivity are retained. Non-covalent functionalization also provides versatility in terms of the types of functional molecules that can be attached, allowing for a wide range of applications.

Both covalent and non-covalent functionalization strategies have their unique advantages and applications. Covalent functionalization provides strong and permanent modifications to the CNT

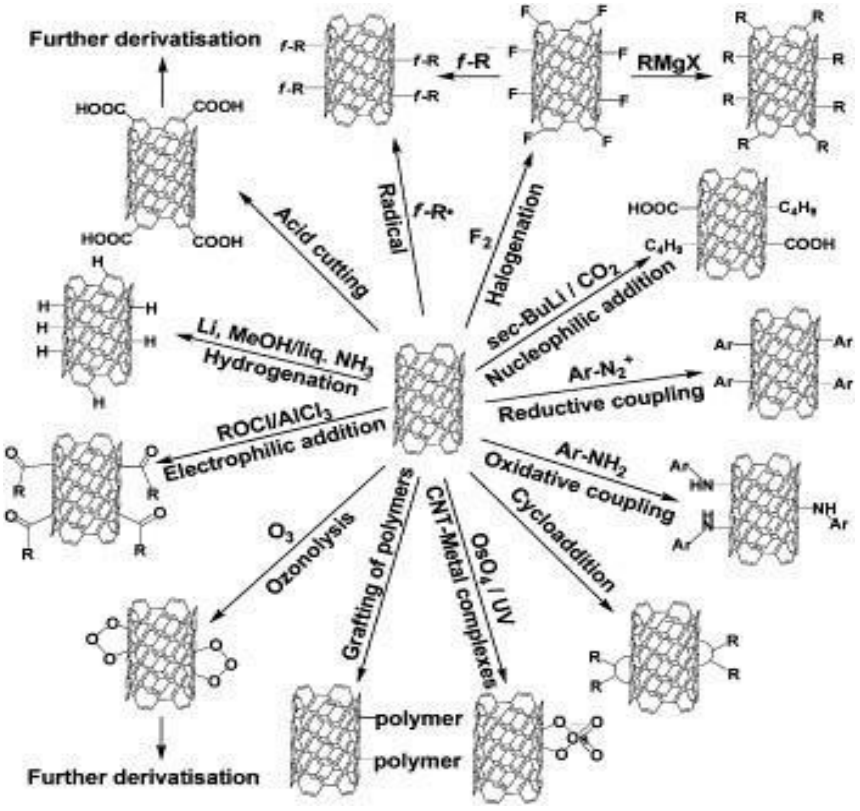

Figure 6 Surface Functionalization of Carbon Nanotubes

surface, offering tailored properties and increased stability. On the other hand, non- covalent functionalization offers reversibility, maintaining the pristine properties of CNTs while allowing for dynamic interactions and easy modification. By utilizing both covalent and non-covalent functionalization approaches, we can create hybrid functionalized CNTs with synergistic properties. This hybrid functionalization combines the advantages of both strategies, providing enhanced functionalities, improved dispersibility, and tailored interactions with various systems.

Polymer Wrapping: CNTs can be functionalized by wrapping them with polymers, such as polyethylene glycol (PEG), polystyrene (PS), or polyvinyl alcohol (PVA). The polymer coating provides stability, dispersibility, and compatibility of CNTs in various solvents or matrices. Polymer wrapping also enables the incorporation of additional functional groups.

Biomolecular Functionalization: CNTs can be functionalized with biomolecules, such as DNA, proteins, or antibodies, to confer specific biological properties. Biomolecular functionalization facilitates targeted delivery, biosensing, or bioimaging applications, opening avenues in biomedical and biotechnological fields.

Hybrid Functionalization: Hybrid functionalization combines different approaches to achieve multi-functional CNTs. For instance, CNTs can be covalently functionalized with specific molecules and subsequently coated with polymers or biomolecules to provide a synergistic combination of properties.

The choice of functionalization method depends on the desired applications and the specific properties required. Functionalized CNTs find applications in areas such as electronics, energy storage, sensing, catalysis, drug delivery, and composite materials. The functionalization process plays a crucial role in tailoring the surface chemistry, dispersibility, and interactions of CNTs, thereby enabling their integration into various systems and enhancing their performance.

2.4. Conductive Polymers

Conductive polymers, also referred to as intrinsically conductive polymers (ICPs), belong to a class of organic materials that exhibit electrical and optical properties resembling those of inorganic semiconductors and metals. There are five well-known types of conductive polymers: polyacetylene, polythiophene, polypyrene, polyphenylene, and polyaniline. These polymers are often referred to as pi-conjugated polymers, indicating that their molecular backbone possesses electrons, resulting in their inherent conductivity. The conductivity values for polyacetylene,

polythiophene, polypyrene, polyphenylene, and polyaniline are 105 S/cm, 100.- 103 S/cm, 2-100 S/cm, 10-3 -103 S/cm, and 10-2 -100 S/cm, respectively.[38]

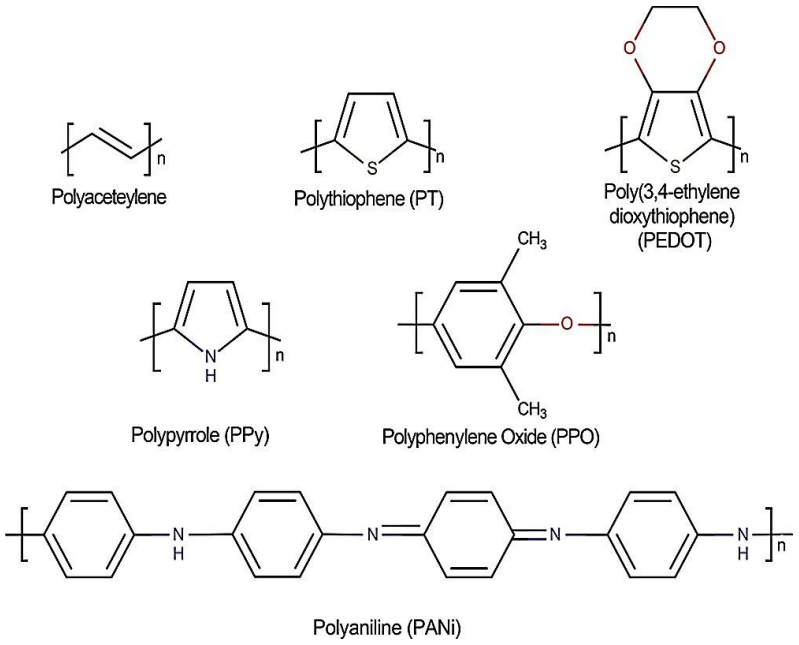

Figure 7 Chemical Structure of five conductive polymers

2.4.1. Polyaniline

PANI (Polyaniline), a conducting polymer, has garnered considerable attention in the field of energy storage due to its unique combination of properties. PANI is renowned for its high electrical conductivity, excellent environmental stability, and low cost. It can undergo redox reactions, providing pseudocapacitive behavior in addition to the double-layer capacitance exhibited by traditional carbon-based materials. This pseudo capacitance arises from the reversible Faradaic redox reactions of PANI, which involve the exchange of ions and protons with the electrolyte. The pseudocapacitive contribution of PANI significantly enhances the overall energy storage capacity of supercapacitors, allowing for higher energy density. Moreover, PANI can be easily synthesized and processed into various forms, including thin films, nanofibers, and composites, making it highly versatile for different electrode architectures. In 1835, polyaniline was known as black aniline. Fritzsche and Letheby conducted studies on the oxidation at Pt electrodes of polyaniline in aqueous sulfuric acid. The discovery of conducting polymers (CPs) occurred in 1960, and among them, polyaniline (PANI) stood out due to its unique properties not found in other CPs.

PANI stood out for its stability, easy chemical or electrochemical synthesis, cost-effectiveness, tunable properties, and remarkable thermal stability. Additionally, PANI exhibits excellent optoelectrical and anti- corrosion properties. The only drawback is its poor solubility in aqueous media and other solvents. However, this challenge has been overcome through the process of doping, which has proven to be an effective solution. Another approach is to create a composite by combining PANI with another polymer to enhance its mechanical properties. Being a p-type conductive material, polyaniline demonstrates outstanding mechanical flexibility and electrical conductivity. Due to its versatile characteristics, it finds wide applications in batteries, supercapacitors, EMI shielding, sensors, and anti-corrosion coatings.[39]

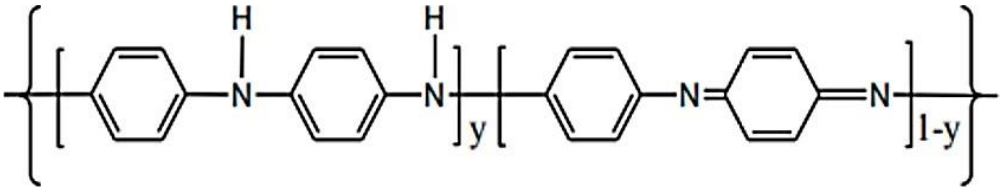

Figure 8 Structure of Polyaniline

2.4.2. Types of Polyaniline

Conductive States

Polyaniline exists in different conductive states, which are highly dependent on its oxidation level. The three main types are:

- Fully Reduced Leucoemeraldine (Insulating state)
- Partially Oxidized Emeraldine (Semi-conducting state)
- Fully Oxidized Pernigraniline (Conducting state)

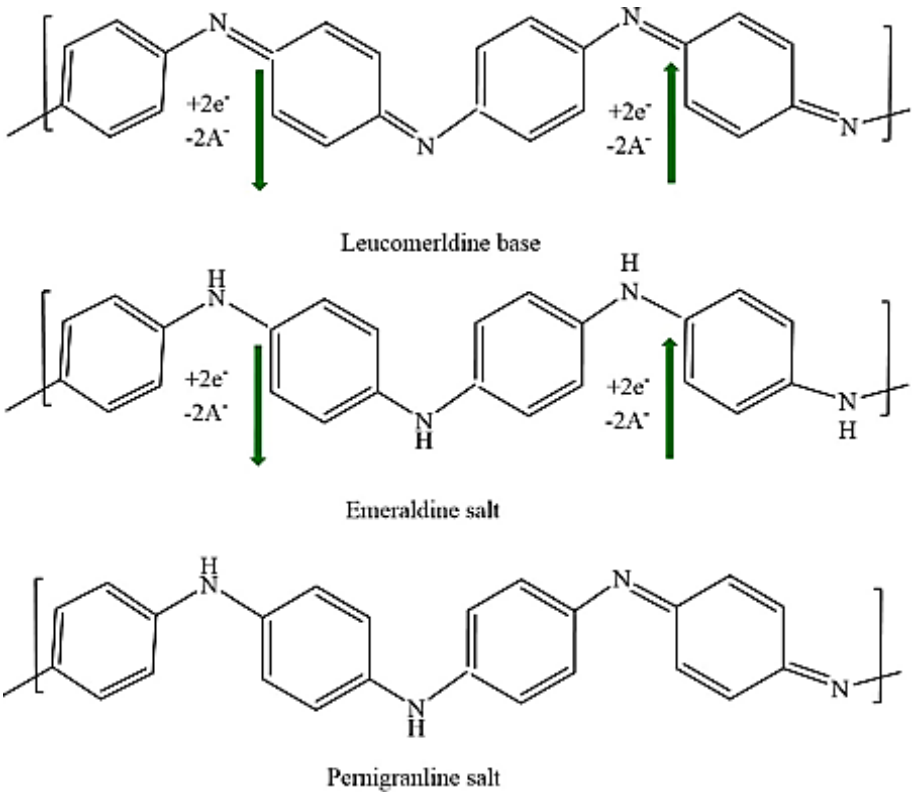

Figure 9 Types of Polyanailine

2.4.3. Doping of PANI

The conductivity and properties of PANI can be significantly enhanced through a process called "doping." Doping involves the introduction of dopant molecules, which can be acids, bases, or other chemicals, into the PANI matrix. This process improves the charge carrier density and overall conductivity of PANI.[40]

2.4.4. Synthesis of PANI

Polyaniline (PANI) can be synthesized using various methods, with the two most common approaches being chemical synthesis and electrochemical synthesis. Both methods allow for the

preparation of PANI with different properties, and the choice of method depends on the desired application and specific characteristics required.[41]

2.4.5. Chemical Synthesis of PANI

This method involves the oxidative polymerization of aniline monomers using different oxidizing agents. Some common oxidants used in this process include ammonium peroxydisulfate (APS), potassium dichromate, or ferric chloride. The polymerization reaction leads to the formation of PANI, and the choice of oxidizing agent can influence the properties of the resulting polymer. Following are the steps for oxidative polymerization:

1. Aniline monomers are dissolved in a suitable solvent (e.g., HCl or H_2SO_4).
2. An oxidizing agent is added to initiate the polymerization reaction.
3. The reaction proceeds, and the PANI is formed as an emeraldine salt.
4. The PANI is then isolated, washed, and dried to obtain the final product.

2.4.6. Electrochemical Synthesis of PANI

In this method, PANI is synthesized through the electrochemical polymerization of aniline monomers using an applied electric potential. The electrochemical synthesis allows better control over the polymerization process and the formation of PANI films or coatings on conductive substrates.

5. Aniline monomers are dissolved in an electrolyte solution containing a suitable dopant (e.g., HCl or H_2SO_4).
6. The electrolyte solution is placed in an electrochemical cell with two electrodes (typically platinum or indium tin oxide) immersed in it.

7. A potential is applied between the two electrodes, initiating the polymerization of aniline monomers on the electrode surface.
8. The PANI film grows on the electrode as the polymerization continues.
9. The electrochemically synthesized PANI film can be carefully removed from the electrode for further characterization or application.

2.4.7. Other Methods

Apart from the chemical and electrochemical methods, some other techniques are also used for PANI synthesis. These methods include:

- Template-assisted synthesis
- Ultrasonication-assisted synthesis
- Micellar polymerization
- In situ polymerization in various matrices

Each method has its advantages and limitations, and researchers select the most appropriate synthesis method based on the specific properties and applications of PANI required for their research or industrial needs.[42]

The combination of $MoSe_2$, CNTS, and PANI in composite materials has shown great potential for advancing the performance of supercapacitors. The synergistic effects of these components result in improved electrochemical properties, stability, and scalability. The incorporation of $MoSe_2$ in the composite enhances the electrical conductivity and provides a stable framework, while CNTS contribute to efficient electron transport and prevent the agglomeration of active materials. The addition of PANI brings pseudocapacitive behavior, further enhancing charge storage capacity. By combining these materials, the resulting composite can achieve high capacitance, rapid charge-discharge rates, excellent cycling stability and improved energy density.[43]

Chapter 3

Materials and Methods

3.1. Chemicals & Materials:

For filtration purposes, Multi Walled Carbon Nanotubes (MWCNTs) were utilized. These MWCNTs were pristine with a carbon content exceeding 94%. The MWCNTs had lengths ranging between 10-15 µm and diameters measuring between 50-85 nm. The chemicals employed in the study included sulfuric acid (H2SO4) with a concentration of 98%, nitric acid (HNO3) with a concentration of 65%, and distilled water. For the filtration process, hydrophilic PTFE (polytetrafluoroethylene) filter paper with a size of 0.2 µm and a diameter of 47mm was used.

The MWCNTs were procured from Graphene Supermarket. PTFE filter paper was purchased from Filter Bio, while the acids were obtained from Merck. Distilled aniline with a concentration of ≥20% was procured from Sigma Aldrich, Germany. Ammonium persulfate (APS) and N, N-dimethyl formamide (DMF) with a concentration of 5% were obtained from Honeywell (USA), and HCl (hydrochloric acid) with a concentration of ≥40% was obtained from AnalaR (UK). Absolute ethanol with a concentration of ≥40% was sourced from RCI Labscan in Thailand. Sodium Molybdate Dihydrate ($Na_2MoO_4.2H_2O$) and Pristine Selenium powder (Se) were obtained from Sigma Aldrich for preparation of $MoSe_2$ Nanospheres. No further treatment/purification were used, and the chemicals were used as received.

3.2. Functionalization of MWCNTS

Initially, 300mg of MWCNTs were dissolved in 9ml of nitric acid (HNO_3) within a round- bottom flask. The flask was equipped with a condenser and placed on a stirring hotplate, maintaining a temperature of 120°C for 12 hours. The reaction was terminated by introducing distilled water into the mixture. The functionalized MWCNTs were subsequently washed multiple times using vacuum filtration with hydrophilic PTFE paper until the pH reached a neutral level, ensuring the elimination of excess acid and by-products. The filter cake was then dried in a drying oven at 80°C for 6 hours

to remove any remaining moisture. As a result of this process, functionalized MWCNTs were successfully obtained, each exhibiting specific properties and functionalities introduced during the reaction. It is crucial to exercise appropriate safety measures when handling nitric acid, given its hazardous nature. [44] Furthermore,

comprehensive characterization and analysis of the functionalized MWCNTs would be necessary to confirm their successful modification and assess their specific properties.

3.3. Synthesis of $MoSe_2$

0.158g of Selenium (Se) powder was dissolved in 5ml of hydrazine and then laid aside for 24 hours. At the same time, 0.206g of Sodium Molybdate Dihydrate ($Na_2MoO_4.2H_2O$) was dissolved in 60ml DI water. Next, the above-mentioned hydrazine hydrate-Se solution was carefully added drop by drop into the sodium molybdate solution [45]. Following this, the resulting mixture, along with a piece of Ni-foam, was placed inside a 100 mL Teflon-lined autoclave. The autoclave was then subjected to a heating process at 180°C for a duration of 48 hours. After the heating period, during the cooling process, the $MoSe_2$ was thoroughly washed with water and ethanol to remove any residual impurities. Finally, the $MoSe_2$ was dried in a vacuum oven to ensure complete removal of any remaining moisture or solvents.

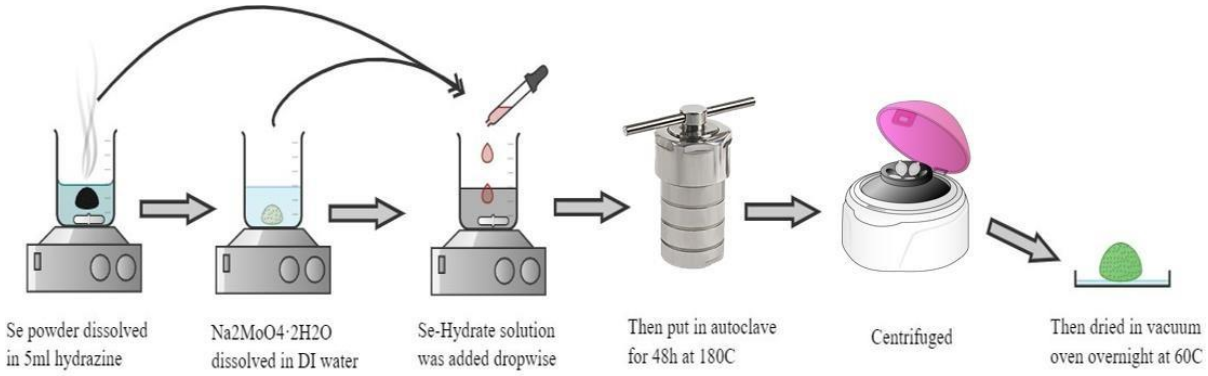

Figure 10 Schematic representation of synthesis of $MoSe_2$

3.4. Synthesis of MWCNTS/$MoSe_2$/PANI Composite

3.4.1. In-Situ Composite

One Pot reaction was followed for the synthesis of in-Situ Hybrid composite. 50mg of MWCNTS along with 1.25g $MoSe_2$ nanospheres were dispersed in 1M aqueous solution of HCL. This mixture is then ultrasonicated for 1 hour. After sonication, 2ml aniline was added in the above solution with continuous stirring in ice bath. Meanwhile, 2.5g of ammonium persulfate (APS) was dissolved in 50ml DI water, this mixture was then added into the above solution with rapid addition (1 drop per second). Once combined, the final mixture was stirred for 5 hours followed by filtration

and washing with ethanol and DI water to remove any impurities. Once washing is completed, the black color residue was dried in a vacuum oven for 12 hours. The obtained material was the final composite and result of fine grinding with mortal and pastel.

3.4.2. Synthesis of Polyaniline

A 1M hydrochloric acid (HCl) solution was prepared by dissolving HCl in 50ml of deionized (D.I) water. In one portion of this 1M HCl solution (25ml), 2.5g of ammonium persulfate (APS) was added and stirred for 20 minutes to dissolve. In another portion of the 1M HCl solution (25ml), 3ml of aniline was added and stirred for 20 minutes to dissolve. An ice bath setup was prepared, and the aniline mixture was poured into a round bottom flask placed in the ice bath. Then, the APS solution was added dropwise (at a rate of one drop per second) into the aniline mixture. During the addition of APS, the mixture's color slowly changed to dark green. The entire reaction was conducted with the ice bath maintained at a temperature around 0-4°C. The dark green solution was stirred for 5 hours at the same temperature range. Following the stirring period, the reaction flask was placed in a refrigerator for 24 hours to allow complete polymerization to occur. After 24 hours, the mixture was taken out of the refrigerator and filtered using ethanol and D.I water to remove any unreacted material. The resulting filtrate was in the form of an emerald, green polyaniline paste. This paste-like filtrate was then dried at 60°C in a vacuum oven. After drying, the material was ground to a fine powder. The final product is the emerald, green polyaniline powder obtained through this process.

3.5. Synthesis of Ex-situ MWCNTS/$MoSe_2$ Composite

Ex-Situ synthesis of MWCNTS/$MoSe_2$ was followed by sonication of MWCNTS in 1M HCL solution for 1 hour. At the same time $MoSe_2$ nanospheres were added in DI water and stirred for 1 hour. After the solution has been stirred, it was added into CNTS solution dropwise. The said mixture was then sonicated for 6 hours. The obtained mixture is now the final ex -situ composite. We have prepared the said ex-situ composite with four different compositions by varying the amount of as prepared $MoSe_2$ decorated onto MWCNTS. The following table shows the name and value of each component used.

Table 2 Comparison of MoSe2/MWCNTs hybrids

Sample name	MWCNTS/$MoSe_2$ Ex-situ Composite	MWCNTS (mg)	$MoSe_2$ (mg)
3C (1:5)	1:1	50	5
3C (1:10)	1:2	50	10
3C (1:15)	1:3	50	15
3C (1:20)	1:4	50	20

3.5.1. Preparation of Ni foam:

Ni foam was used as a substrate for deposition of functionalized CNTS, PANI, MWCNTS/PANI/$MoSe_2$(In-Situ), $MoSe_2$, $MoSe_2$/ CNTS (Ex-Situ Hybrid Composite).

3.5.2. Cleaning of Ni Foam

Nickel foam was cleaned by sonicating in ethanol, Distilled water, Acetone and HCL for 10 minutes respectively. The nickel foam was cut in 1x1 cm of area where we can then drop cast the desired material to be tested through three – electrode as shown in the figure.

Chapter 4

Characterization

4.1. Instrumentation and Measurements

The samples' morphological studies were examined using various techniques. Scanning Electron Microscopy (SEM) was employed, utilizing a JEOL JSM-6490A instrument from Tokyo, Japan. Elemental analysis was carried out through SEM by using a combined EDAX EDS probe. Structural information was analyzed using X-ray diffraction (XRD) on a Seimens D5005 STOE & Cie GmbH instrument from Darmstadt, Germany. The XRD measurements were taken at an angle (2θ) ranging from 10° to 80°. For the analysis of FTIR (Fourier Transform Infrared) spectra, a PerkinElmer, SpectrumTM100 spectrophotometer was used. The analysis involved potassium bromide pellets along with dried powder samples. Raman spectra were collected using a BWS415-532S-iRaman instrument manufactured by BW TEK INC, located in Newark, NJ, USA. For electrochemical measurements we use the Gamry Echem Analyst which is a powerful software package used in conjunction with Gamry Instruments' potentiostats/galvanostats for electrochemical testing and analysis. [46]

The Gamry Echem Analyst software is designed to work seamlessly with a wide range of Gamry potentiostats and galvanostats, such as the Reference 3000, Interface 5000, and Interface 1000 series, among others. The software allows for precise and efficient data acquisition in various electrochemical techniques, including cyclic voltammetry, chronoamperometry, chronopotentiometry, impedance spectroscopy, and more. Users can set up and control various electrochemical experiments through an intuitive graphical interface. The software provides flexibility in defining experimental parameters, such as scan rates, potential ranges, and sampling intervals. Gamry Echem Analyst provides real-time data visualization during experiments, allowing researchers to monitor and analyze the results as they are being collected. For impedance spectroscopy measurements, the software provides the capability to plot Nyquist and Bode plots, extract equivalent circuit parameters, and perform fitting for impedance data. Gamry Echem Analyst allows users to create complex experiment sequences by combining multiple techniques,

making it ideal for studying various electrochemical processes in a single experiment. Users can export data to various formats, such as Excel, CSV, or ASCII files, for further analysis in external software. The software also supports generating comprehensive reports summarizing experimental results.

4.2. Scanning Electron Microscope

Scanning electron microscopy (SEM) is a widely utilized technique for high-resolution imaging of materials, revealing details that are not visible to the naked eye. By employing a beam of high-energy electrons to scan the surface of an object, SEM magnifies its features and generates an image with exceptional clarity. This microscope operates at a smaller wavelength, enabling the visualization of even the most minute structures. With a resolution up to one million times the original size of the object, researchers worldwide employ SEM to achieve micro and nano-level resolutions. Compared to the human eye with a resolution of 200 µm, SEM surpasses it by a factor of 1000, reaching 0.2 µm. Consequently, if two features of a material are smaller than 0.2 µm, they would appear indistinguishable under this microscope. The remarkable resolution of SEM is attributed to the utilization of an electron beam accelerated by a voltage of 100kV.

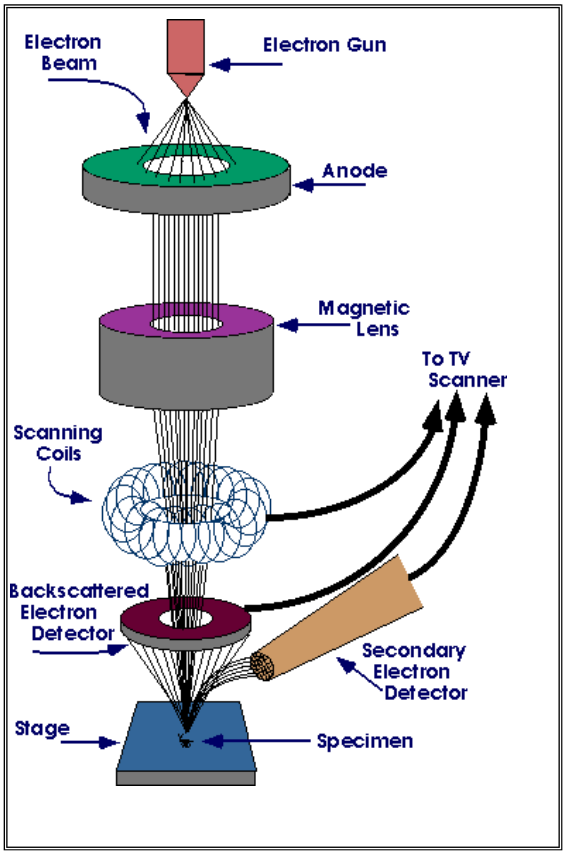

Figure 11 Schematic Representation of scanning electron microscope

SEM can resolve both conductive and non-conductive materials, and the inclusion of an energy-

dispersive X-ray spectroscopy (EDS) detector allows for elemental analysis of the sample. It provides both quantitative and qualitative information about the material under examination. Typically, samples are mounted on stubs within the sample chamber and are often coated with a thin layer of gold for improved imaging quality.

The cathode assembly, known as the electron gun, is connected to a high-voltage power cable ranging from 30kV to 40kV. This assembly generates and accelerates electrons through the chamber. The four types of electron guns commonly used are Schottky field emission, cold field emission, LaB6 emitter, and tungsten filament. After electron generation, an electron energy spread occurs, where the source operating at an accelerating voltage of 20 kV emits most electrons at an energy of 20 keV. Electrons with varying velocities are captured by different electron lenses at distinct planes. Clearer images are produced by capturing electrons with lower energy spreads, as they are easier to collect. Subsequently, the electromagnetic lenses focus the beam into a probe, which scans the material area in a raster pattern. This probe is then reconverged by the condenser lens, forming a fine probe through the objective lens. The backscattered electrons' energy emitted from the sample is detected by a backscattered electron detector. The entire setup operates under vacuum conditions. The secondary detector captures dislodged electrons, and the resulting image on the screen is formed by amplifying and displaying the signals emitted and received by the detector, creating an interface with the sample.

4.3. Xray Diffraction:

X-ray diffraction (XRD) is a powerful analytical technique widely utilized in material science and solid-state physics for the characterization of crystalline materials. By examining the scattering of X-rays from a sample, XRD provides valuable insights into its crystal structure, lattice parameters, phase composition, grain size, and microstructural features. This report aims to provide a comprehensive overview of XRD, including its principles, instrumentation, data analysis, and applications.

4.3.1. Principles of X-ray Diffraction

XRD is based on the phenomenon of X-ray diffraction, which occurs when X-rays interact with the regular arrangement of atoms within a crystalline material. The diffraction pattern obtained from the scattered X-rays contains information about the spatial arrangement of the crystal lattice and the interatomic distances. Bragg's law, expressed as

$$2d_{hkl} \times \sin\theta_{hkl} = \lambda$$

It relates the diffraction angle (2θ) of a particular reflection to the interplanar spacing (d_{hkl}) of the crystal lattice and the X-ray wavelength (λ).

4.3.2. Instrumentation

XRD experiments are typically conducted using a specialized instrument known as an X-ray diffractometer. The key components of a diffractometer include an X-ray source, a sample holder, a goniometer, and a detector. The X-ray source emits monochromatic X-rays, often generated by a tube containing a target material such as copper or cobalt. The sample holder securely positions the sample, while the goniometer allows precise rotational and angular movements. The detector captures the diffracted X-rays and produces a diffraction pattern.

4.3.3. Data Analysis

The diffraction pattern obtained from the detector is in the form of intensity versus diffraction angle (2θ). Data analysis techniques involve identifying and indexing the diffraction peaks, determining their positions, and calculating the corresponding interplanar spacings. The qualitative and quantitative analysis of the diffraction data is performed using specialized software, which compares the experimental data with established databases of known crystal structures.

4.3.4. Applications of XRD

XRD finds widespread applications in various fields, including materials science, solid-state chemistry, geology, pharmaceuticals, and metallurgy. It is extensively used to determine the crystal structure and phase identification of materials, assess the quality of crystalline samples, investigate crystallographic changes under external stimuli (temperature, pressure, etc.), analyze residual stresses and texture, and study phase transformations and amorphous materials. XRD is also employed for the characterization of thin films, nanomaterials, and complex multicomponent systems.

X-ray diffraction is a versatile and indispensable technique for the structural characterization of crystalline materials. Its non-destructive nature, high sensitivity, and wide range of applications make it an essential tool for researchers and scientists in numerous fields. The ability to obtain detailed information about crystal structures and properties plays a crucial role in understanding material behavior, designing new materials, and advancing technological innovations.

In summary, XRD provides valuable insights into the atomic arrangement and crystallographic properties of materials, enabling researchers to deepen their understanding of structure- property relationships and develop novel materials with tailored properties.

4.4. Fourier Transform Infrared Spectroscopy: A Window into Molecular Vibrations

Fourier Transform Infrared (FTIR) spectroscopy is a powerful analytical technique widely used in chemistry, materials science, and various scientific disciplines. It provides valuable insights into the molecular structure, composition, and functional groups present in a sample by analyzing the interactions between infrared (IR) radiation and the sample's molecules. This report aims to provide a comprehensive overview of FTIR spectroscopy, including its principles, instrumentation, data analysis methods, and applications.

FTIR spectroscopy is based on the principle that molecules absorb specific frequencies of infrared light, corresponding to the vibrational modes of their chemical bonds. When IR radiation passes through a sample, certain wavelengths are absorbed, resulting in characteristic absorption bands in the spectrum. These absorption bands provide information about the chemical bonds, functional groups, and overall molecular structure of the sample. FTIR spectra are typically displayed as a plot of percent transmittance or absorbance against wavenumber, which is the reciprocal of the wavelength. The spectrum consists of a series of peaks or bands, each corresponding to a specific vibrational mode in the molecule can be assigned to specific functional groups or molecular vibrations using spectral libraries, databases, or expert knowledge. Quantitative analysis can be performed by measuring the peak intensities and comparing them to calibration standards or using specific peak areas.

4.5. Cyclic Voltammetry: Probing Electrochemical Behavior and Analyzing Redox Processes

Cyclic Voltammetry (CV) is a widely used electrochemical technique that provides valuable information about the redox behavior, electrochemical processes, and kinetic properties of electroactive species in a solution. This report aims to provide a comprehensive overview of

cyclic voltammetry, including its principles, experimental setup, data analysis methods, and applications. A typical CV experiment involves the use of a potentiostat, which controls the applied potential, measures the resulting current, and maintains the desired experimental conditions. The working electrode is immersed in the electrolyte solution, and the potential is swept between a starting and ending potential at a controlled scan rate. The resulting current is recorded, and the resulting cyclic voltammogram is plotted as current density (or current) versus applied potential. Cyclic voltammograms provide valuable information about the redox processes occurring at the working electrode. The shape and position of the peaks in the voltammogram can indicate the nature of the electrochemical reactions, such as oxidation or reduction processes. By analyzing the peak potentials and peak currents, electrochemical parameters such as the formal potential, peak separation, and electron transfer coefficients can be determined. Moreover, CV data can be used to calculate the diffusion coefficient, rate constant, and other kinetic parameters.

Furthermore, cyclic voltammetry is employed in the investigation of electrochemical reaction mechanisms, analysis of redox-active species, and determination of electrochemical parameters for various applications. Cyclic voltammetry, including its principles, experimental setup, data analysis methods, and applications. Cyclic voltammetry is based on the measurement of current as a function of applied potential. A three-electrode setup is typically used, consisting of a working electrode, a reference electrode, and a counter electrode. The working electrode is the site where the electrochemical reaction occurs, and the reference electrode provides a stable reference potential. By sweeping the applied potential linearly over time, cyclic voltammetry allows the observation of redox reactions, determination of electrochemical parameters, and analysis of the kinetics and thermodynamics of the electrochemical processes. A typical CV experiment involves the use of a potentiostat, which controls the applied potential, measures the resulting current, and maintains the desired experimental conditions. The working electrode is immersed in the electrolyte solution, and the potential is swept between a starting and ending potential at a controlled scan rate. The resulting

current is recorded, and the resulting cyclic voltammogram is plotted as current density (or current) versus applied potential. Furthermore, cyclic voltammetry is employed in the investigation of electrochemical reaction mechanisms, analysis of redox-active species, and determination of electrochemical parameters for various applications.

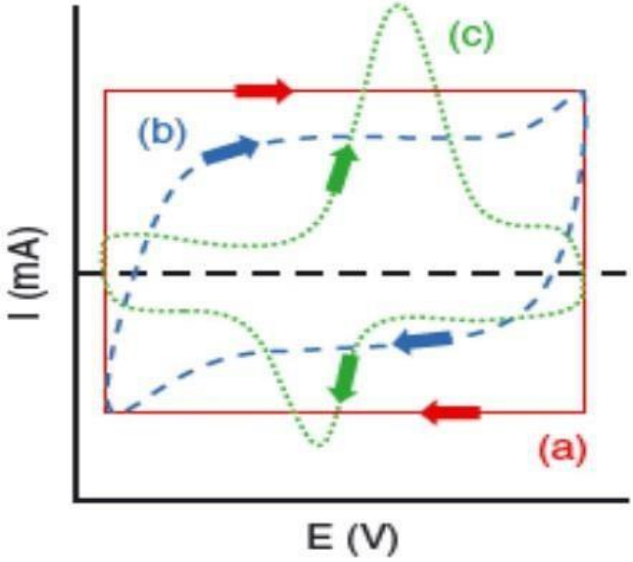

Figure 12 CV Plot for (a) Ideal supercapacitor with rectangular shape (b)EDLC with rectangular shape (c)Pseudo capacitor with oxidation and reduction peaks

4.6. Cyclic Charge-Discharge: Investigating Energy Storage and Performance of Electrochemical Systems

Cyclic charge-discharge is an essential technique used to evaluate the energy storage capabilities, performance, and efficiency of electrochemical systems, particularly in energy storage devices such as batteries and supercapacitors. This report aims to provide a comprehensive overview of cyclic charge-discharge, including its principles, experimental setup, data analysis methods, and applications.

Cyclic charge-discharge involves the repeated cycling of an electrochemical cell or device between charging and discharging states. During the charging process, energy is stored in the electrochemical system by the conversion of electrical energy into chemical potential energy. The discharging process, on the other hand, involves the release of stored energy as electrical energy.

This cycling process allows for the evaluation of the energy storage capacity, efficiency, and stability of the electrochemical system.

A typical cyclic charge-discharge experiment requires an electrochemical cell or device, a power source, and monitoring equipment. The electrochemical cell consists of electrodes, electrolyte, and separators. The electrodes are typically made of active materials capable of storing and releasing charge. The electrolyte facilitates the ion transport between the electrodes, while the separators prevent direct contact between the electrodes. The cell is connected to a power source that applies a voltage or current to charge or discharge the system. During cycling, the current and voltage are monitored, and the data is recorded for analysis.The data obtained from cyclic charge-discharge experiments is typically analyzed to evaluate the energy storage performance and characteristics of the electrochemical system. Parameters such as capacity, efficiency, energy density, power density, and voltage profiles are calculated and analyzed. The cyclic stability and degradation of the system over multiple cycles are also assessed. Various mathematical models and algorithms can be applied to analyze the data and extract valuable insights regarding the system's behavior and performance.

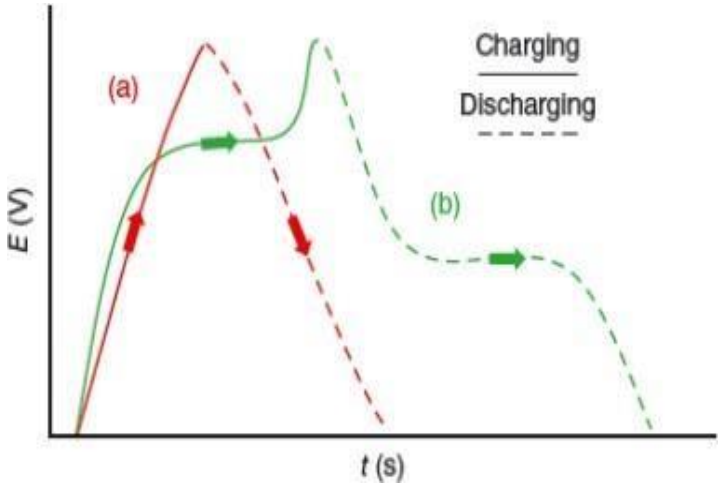

Figure 13 GCD Curves

4.7. Electrochemical Impedance Spectroscopy (EIS)

Electrochemical Impedance Spectroscopy (EIS) is a powerful technique used to analyze the electrical behavior of electrochemical systems. It provides valuable information about the complex impedance of the system as a function of frequency, allowing for the investigation of

various electrochemical processes. This report aims to provide a detailed overview of EIS, including its principles, experimental setup, data analysis methods, and applications. EIS is based on the measurement of the impedance of an electrochemical cell or system over a range of frequencies. The impedance is a complex quantity that includes both resistance (real component) and reactance (imaginary component). By applying an AC voltage or current signal with a known frequency to the system, the resulting current or voltage response is measured. This response is used to calculate the impedance and construct an impedance spectrum, which provides insights into the system's electrochemical behavior. To perform EIS, an electrochemical cell or system is required, along with a potentiated/galvanostatic, a frequency response analyzer, and appropriate software for data acquisition and analysis. The cell typically consists of working, reference, and counter electrodes immersed in an electrolyte. The potentiostat/galvanostat controls the voltage or current applied to the cell, while the frequency response analyzer measures the resulting current or voltage response over a range of frequencies discharging states, important parameters related to capacity, efficiency, power density, and stability can be determined. This information is crucial for the development and optimization of energy storage devices, leading to advancements in various fields such as renewable energy, electric vehicles, and portable electronics. Continued research and refinement of cyclic charge- discharge techniques will contribute to the ongoing progress in energy storage technologies. In conclusion, cyclic charge-discharge is a vital tool for assessing the energy storage performance and characteristics of electrochemical systems. Its application in batteries, supercapacitors, and other energy storage devices allows for the evaluation and improvement of their efficiency, stability, and cycle life. With the growing demand for efficient and sustainable energy storage solutions, cyclic charge-discharge experiments will continue to play a pivotal role in advancing energy storage technologies.

EIS is used to evaluate the performance and degradation of batteries, fuel cells, and supercapacitors, aiding in the development of more efficient energy storage systems. Corrosion Analysis: EIS is employed to study and mitigate corrosion in various industries such as oil and gas, marine, and infrastructure, helping to extend the lifespan of materials.

Coatings and Paints: EIS assesses the protective properties of coatings and paints, ensuring their effectiveness in preventing corrosion or degradation. Biosensors: EIS is utilized in the development of biosensors for medical and environmental applications, enabling the detection of biomolecules with high sensitivity . EIS helps understand and optimize the electrochemical processes within fuel cells, contributing to the development of clean energy technologies. Materials Science: EIS is applied to investigate the electrical properties of materials, including semiconductors and polymers, aiding in the development of new materials with specific properties.

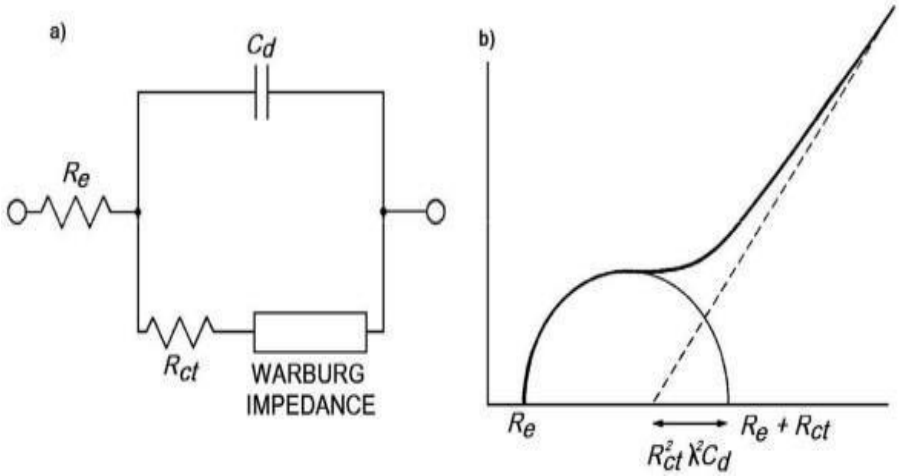

Figure 14 (a)Equivalent circuit Diagram (b) Nyquist plot

Chapter 5

Results and Discussion

5.1. Xray diffraction

X-ray diffraction (XRD) analysis employing Copper K Alpha radiation was conducted to investigate the composite material. The scan range encompassed 10 to 90 degrees, generating XRD peaks as depicted in Figure. The composite primarily consisted of Carbon Nanotubes (CNTs), with a minority presence of Molybdenum Selenide ($MoSe_2$). Due to the fusion of $MoSe_2$ within the carbon hexagonal lattice, a slight shift in the peak positions was observed. Increasing quantities of $MoSe_2$ resulted in a notable shift towards lower angles, indicative of a semi-distorted structure. Moreover, the intensity of CNT peaks exhibited an increment, while the intensity of $MoSe_2$ peaks diminished. These findings affirm our hypothesis of $MoSe_2$ merging with the Carbon Nanotubes' structure, establishing a basis for their interfacial interaction. The X-ray diffraction (XRD) analysis of the functionalized MWCNTs exhibits the expected peaks at 2θ angles of 26.2°, 42.2°, 53.9°, and 77.1°, which correspond to the crystallographic planes (002), (100), (004), and (110), respectively. These assignments are in accordance with the data from JCPDs card 75-1621.

Notably, the presence of a strong and intense peak at 23° is a clear indicator of the functionalization of the MWCNTs by acids. This heightened intensity suggests structural modifications in the MWCNTs due to the acid treatment, confirming the success of the functionalization process. A noteworthy distinction can be observed between the XRD peaks (Graph - 3) of Carbon Nano Tubes (CNT) and Pristine CNT. While they share similar peaks, a notable difference arises at the 45-degree angle, where an additional plane corresponding to (101) is present. This additional plane signifies the existence of another phase, distinct from that of the CNT structure. The presence of this new phase suggests a divergence or variation in the crystalline nature of the Pristine CNT, highlighting its unique characteristics compared to regular CNT samples. The (002) and (100) planes of carbon nanotubes demonstrate a remarkable ability to dissolve a significant portion of the MoSe2 within their structure. Through a process akin to dissolution, the MoSe2 seamlessly integrates itself into the intricate lattice of the carbon nanotubes, resulting in a transformative phenomenon. The functionalized Carbon Nano Tubes (MWCNTs) exhibit two prominent peaks at angles of 23 and 39 degrees, indicating a stable

structure devoid of other phases. The intensity and distinctness of these peaks serve as indicators of the CNTs' structural integrity. Conversely, the XRD analysis of PANI (polyaniline) may not reveal prominent peaks due to its lower crystallinity. However, the presence of the (200) plane is discernible. The broadening of peaks can be attributed to the lower crystallinity and fusion of the (011), (020), and (200) planes within PANI.

Although the MoSe2 hexagonal structure's peaks are visible in the XRD analysis, their intensity is relatively low. This diminished intensity can be attributed to the formation of MoSe2 nanoparticles, which exhibit significantly lower crystallinity. Nevertheless, the presence of the MoSe2 structure is confirmed through XRD techniques. The X-ray diffraction (XRD) analysis of pure PANI reveals distinct peaks at 2θ angles of 15.5°, 20.7°, and 25.5°. These peaks are associated with the crystallographic planes (121), (113), and (322), respectively, as confirmed by comparison with the data from JCPDS card no. 72-0634. This alignment with established reference data corroborates the crystallographic structure of pure PANI. At the bottom of the picture, the XRD analysis of the composite comprising CNTs, PANI, and MoSe2 is presented. The direct alignment of peaks indicates that the structure has not undergone significant solid solution formation, with the individual entities within the composite retaining their distinct crystal structures. Notably, all planes can be clearly visualized in figure 15.

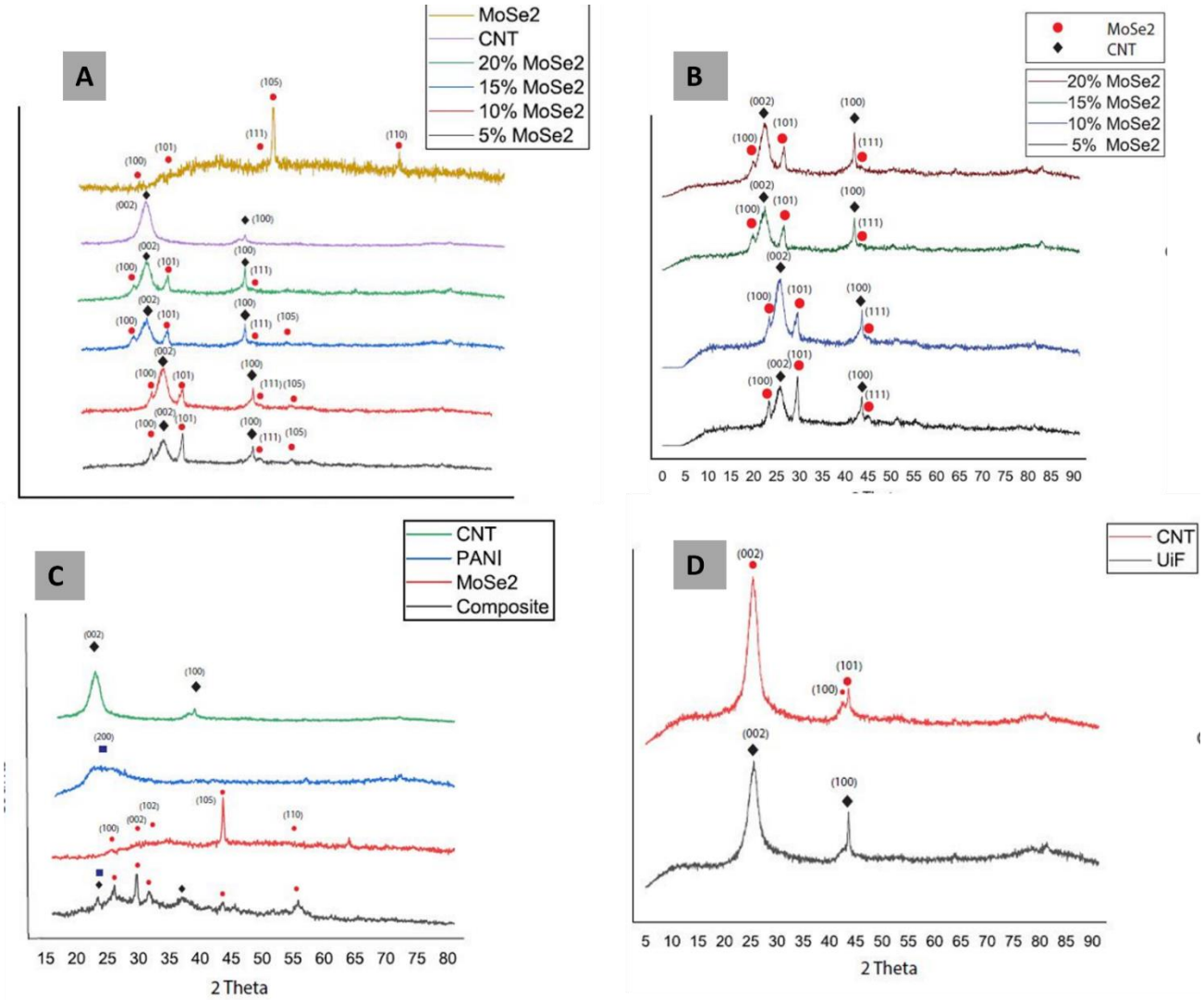

Figure: 15 XRD Patterns of (a)MoSe2 & MWCNTs (b)Ex-situ MWCNTS/MoSe2 (c) MWCNTS/MoSe2-PANI (D) Pristine and Functionalized CNTs

5.2. Fourier Transformation Infrared Spectroscopy

The spectral characteristics of the multi-walled carbon nanotubes (MWCNTs), both functionalized and non-functionalized, exhibit distinctions. Following functionalization, the prominent peak at 2853.55 cm^{-1} corresponds to the stretching vibrations of C-H bonds, indicative of the presence of hydrocarbons or organic moieties. At 2319.10 cm^{1}, a distinct peak is observed, suggesting the presence of C≡C triple bonds, characteristic of alkynes. The peak at 1102.41 cm^{-1} is attributed to the stretching vibrations of C-O bonds, indicating the potential existence of oxygen-containing functional groups. Furthermore, the peak observed at 800.39 cm^{-1} is consistent with C-H out-of-plane bending vibrations, common in hydrocarbon structures. The absorbance registered within the range of 600 - 2000 cm^{-1} corresponds to specific molecular vibrations. The spectral region between 600 and 925 cm^{-1} is indicative of O-Mo-O bonds. A peak at 1411 cm^{-1} is associated with Se-O bonds. Additionally, a noteworthy absorption band at 1646 cm^{-1} is linked to COOH functional groups. The observed FTIR peaks for PANI in this analysis align well with previously reported literature. Here's a summary of the identified peaks and their associated vibrational modes: The peak at 794 cm^{-1} corresponds to the aromatic C-H out-of-plane bending vibration. At 1105 cm^{-1}, the peak is indicative of the aromatic C-H in-plane bending vibration. Peaks at 1294 cm^{-1} and 1256 cm^{-1} are attributed to the C-N stretching vibrations of the secondary aromatic ring of PANI. The peaks at 1465 cm^{-1} and 1512 cm^{-1} represent the C=C stretching vibrations of the Benzenoid (B) and Quinoid (Q) rings, respectively, in the PANI structure. The peak at 3433 cm^{-1} is associated with the N-H stretching vibration of secondary amine groups in PANI. These findings are consistent with the established literature on PANI's FTIR spectra, reaffirming the structural characteristics of the PANI component within your MoSe2/PANI/MWCNTs composite. he PANI/MWCNT $MoSe_2$ composite, synthesized in-situ, exhibits noteworthy spectral features: A prominent, sharp, and intense spectral band at 616 cm^{-1} is attributed to the characteristic absorption of $MoSe_2$.There is an observed merging of the bands at 1650 cm^{-1}, indicating the presence of intermolecular interactions between MoSe2 nanoparticles and PANI. Additionally, a distinct conductive peak at 3428 cm^{-1} is evident in the composite. The peaks for $MoSe_2$ NPs can be seen in MM (1:3) and (1:4) and show little to no peak in MM (1:1) and MM (1:2), which also shows that by increasing the amount of CNTs in composite, the peaks intensity of CNTs increases. These spectral characteristics provide valuable insights into the composition and structural properties of the PANI/MWCNT MoSe2 composite.

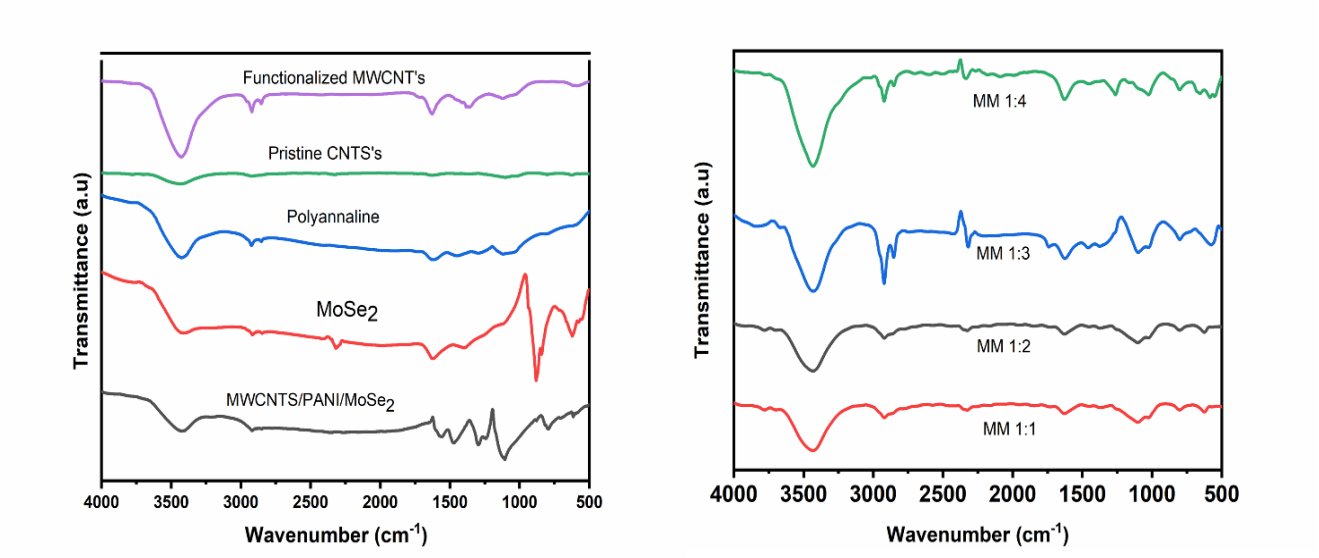

Figure 16: FTIR Graphs for (a)Functionalized MWCNTs, Pristine CNTs, $MoSe_2$, PANI & PANI-MWCNTs/$MoSe_2$ (b)$MoSe_2$/MWCNTs Hybrids (1:1 - 1:4)

5.3. RAMAN Analysis:

Raman analysis serves as a powerful tool for discerning the vibrational characteristics of compounds or composites, offering a unique insight into their chemical nature, bonding, and functional groups. This analysis involves laser light with a wavelength of 532 nm, which serves as a distinctive signature for specific materials or composites. Raman scattering, triggered by the interaction of light with the material, results in the emission of rays with a slight shift in wavelength. This shift aligns with the vibrational modes or energy levels of the bonds present within the material. In the case of $MoSe_2$, the Raman spectrum exhibits five major peaks at 149.0 cm^{-1}, 237.6 cm^{-1}, 1344.6 cm^{-1}, 1582 cm^{-1}, and 2701.6 cm^{-1}. These peaks are characteristic of $MoSe_2$, confirming the absorption of light by the bonds within the material. Similarly, pristine CNTs display three major peaks at 1349.6 cm^{-1} (D band), 1582.7 cm^{-1} (G band), 1387 cm^{-1}, and 2697.7 cm^{-1}. The presence of the G band at 1582.7 cm^{-1} confirms the existence of CNTs, with a slight increase in intensity observed at the D band peak of 1349.6 cm^{-1} in the Raman spectra. In the case of PANI, the Raman spectrum exhibits ten peaks at 163.8 cm^{-1}, 411.9 cm^{-1}, 567.9 cm^{-1}, 816.1 cm^{-1}, 1172.2 cm^{-1}, 1241.2 cm^{-1}, 1339.6 cm^{-1}, 1401.9 cm^{-1}, 1558.6 cm^{-1}, and 1594.7 cm^{-1}. These peaks are indicative of the functional groups and bonding within PANI, with the Raman shift

intensity reflecting the absorption of light by the vibrational energy levels of its constituent bonds. The D-band (~1350 cm^{-1}) and G-band (~1580 cm^{-1}) are associated with structural disorders and the graphitic nature of carbon materials, respectively. The G-band (~2660 cm^{-1}) represents the first overtone of the D mode peaks. The ID/IG ratio serves as an indicator of structural defects in graphitic carbons, often caused by chemical modifications. Notably, the C–N•+ stretching vibration of semiquinone radicals at 1331 cm^{-1} confirms PANI doping, indicating its conducting form. Additional peaks at 1405, 1478, and 1595 cm^{-1} correspond to C–C stretching, C=N stretching, and C=C stretching of the quinoid ring, respectively. Smaller peaks at 1221 and 1251 cm^{-1} are associated with C–N stretching in the benzenoid ring and C–N•+ of semiquinone radicals, respectively. In the Raman spectra of the PANI/MWCNT-MoSe2 composite, a noteworthy observation is the presence of additional peaks at approximately 249.4 cm^-1. These peaks, in conjunction with those of MWCNTs and PANI, collectively define the composite's spectral signature. Moreover, when examining the Raman spectra of MM (1:1) to (1:4) hybrids, a consistent and distinct peak emerges at 249.4 cm^-1, alongside the D-band (~1350 cm−1) and G-band (~1580 cm−1) associated with MWCNTs. However, the behavior of the composites diverges significantly. Apart from the Raman spectra characteristics typically associated with polyaniline, the increased concentration of MoSe2 nanoparticles exerts a notable influence. This influence is evidenced by a broadening and intensified peak around 249.4 cm^-1, signifying the presence of interactions between the polymer and the hybrid material. In summary, the Raman analysis reveals distinct peaks for MoSe2, CNTs, and PANI, confirming their presence and structural characteristics. Furthermore, the composite of CNTs/MoSe2 exhibits combined peaks that align with the signatures of both materials, providing compelling evidence of its composite nature.

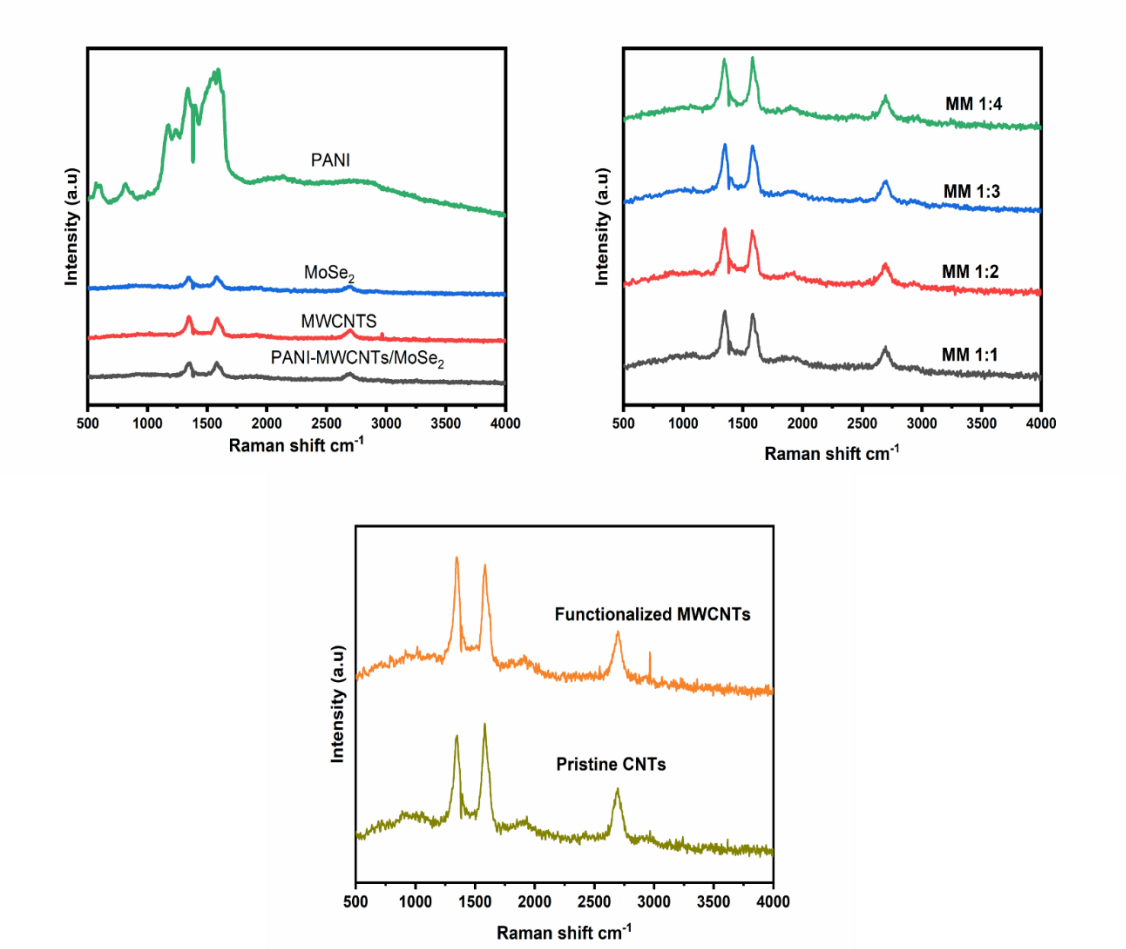

Figure 17: Raman Spectra of (a) MWCNTS/$MoSe_2$/PANI, $MoSe_2$, PANI & MWCNTS (b) MWCNTs/$MoSe_2$ hybrid composites (c) Pristine & functionalized CNTs

5.4. SEM (Scanning Electron Microscopy)

The base material used for the experiments was functionalized Multiwalled Carbon Nanotubes (MWCNTs). The Scanning Electron Microscopy (SEM) results in Figure 18 (a) show the MWCNTs after undergoing acid functionalization, which leads to the roughening of the nanotubes and provides attachment sites for functional groups. The $MoSe_2$ nanoparticles that were synthesized were found to have relatively uniform sizes, with an average size of 39 nm, as seen in Figure 18 (d). In the MWCNTs- $MoSe_2$ NPs (Ex-situ) hybrid, small $MoSe_2$ nanoparticles are observed to be decorated on the MWCNTs. Among all the compositions of MWCNTs- $MoSe_2$ NPs hybrids, 20% $MoSe_2$ shows the highest number of $MoSe_2$ NPs attached onto the surface of MWCNTs.

Pure polyaniline forms a fine network of polymer connecting the tubes. In PANI/MWCNT-$MoSe_2$ hybrid (In-situ), polyaniline is deposited on the hybrid structure, as seen in Figure 18. In the MWCNTs- $MoSe_2$ Nanospheres (Ex-situ) hybrid, tiny $MoSe_2$ nanoparticles are intricately attached to the surface of MWCNTs. Among all the different compositions of MWCNTs- $MoSe_2$ Nanospheres hybrids examined, the MM (1:4) composition demonstrates the highest level of $MoSe_2$ NPs adherence onto the MWCNTs' surface.

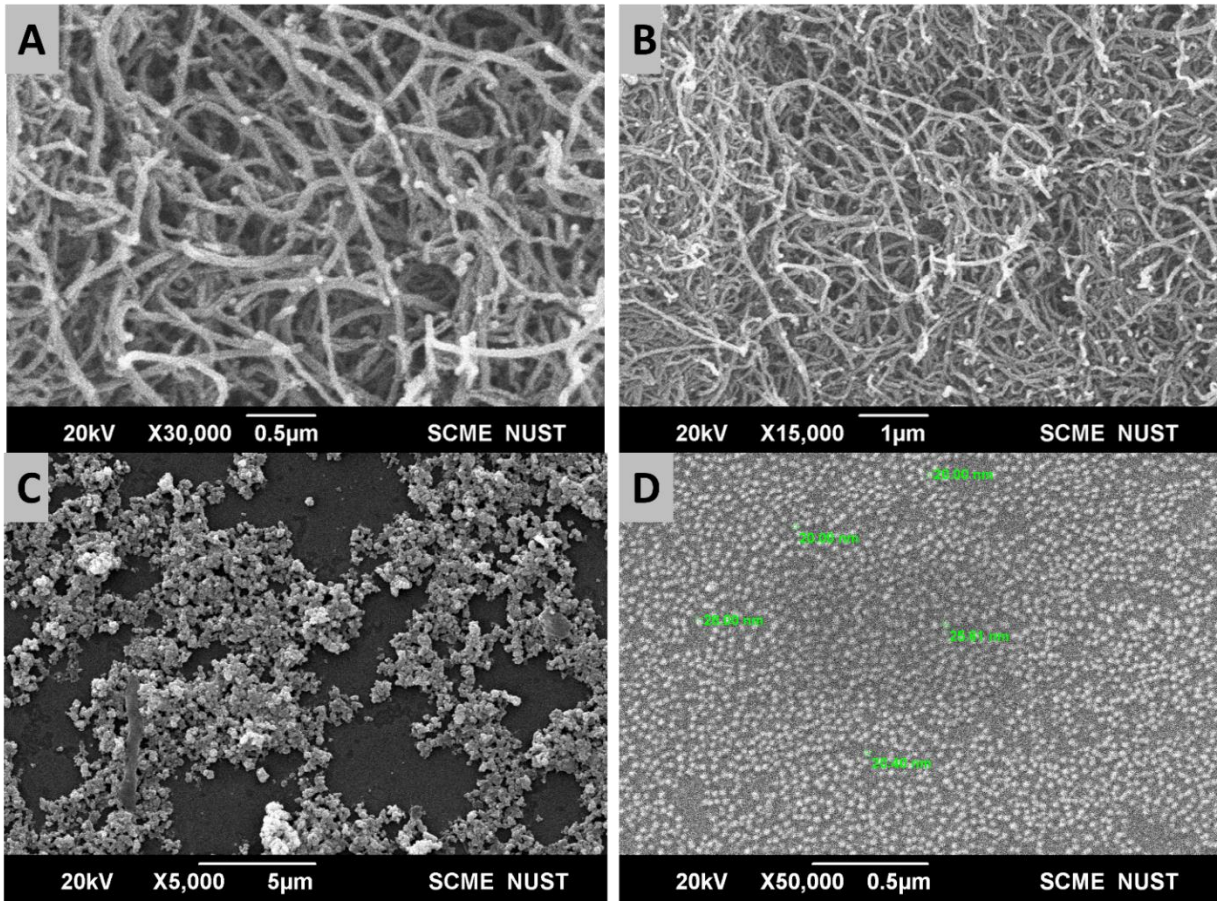

Figure 18: SEM results of (a) funct..MWCNTs (b) Pristine CNTs (c) PANI (d)$MoSe_2$ Nanospheres

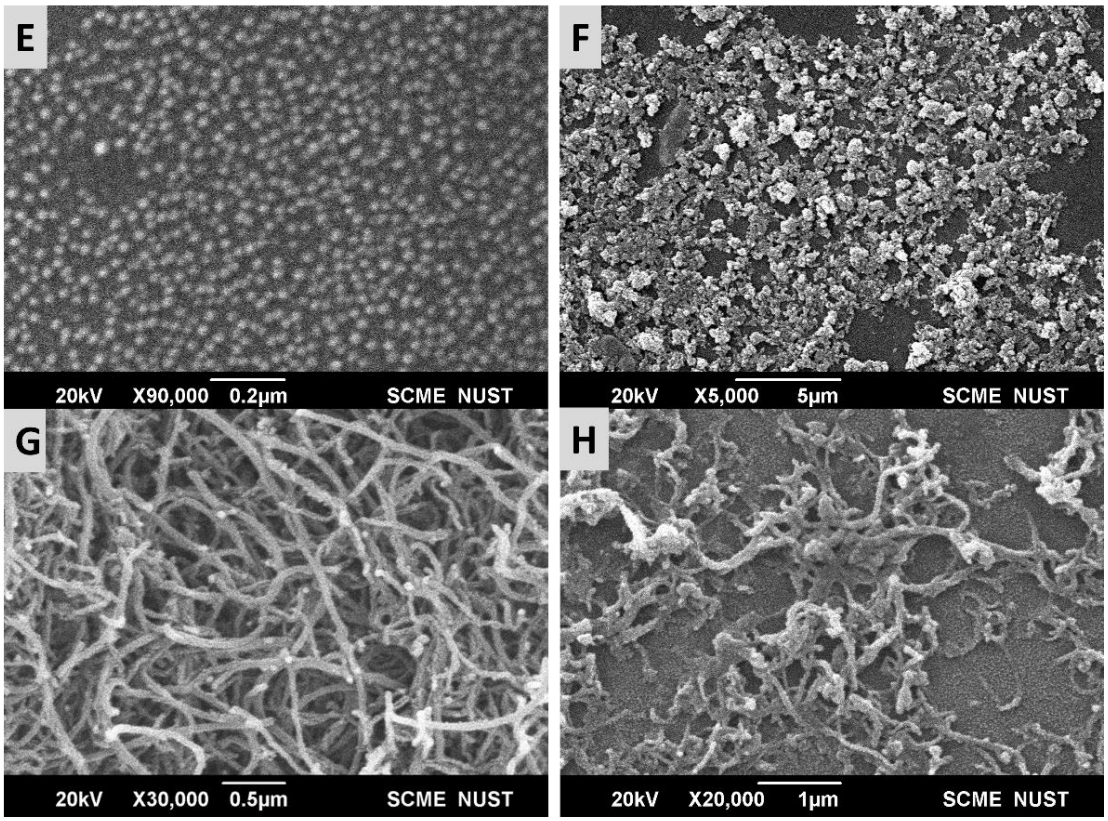

Figure 19: SEM results for (a) $MoSe_2$ Nanospheres (b) PANI (c)MWCNTs (d)PANI-MWCNTs/$MoSe_2$

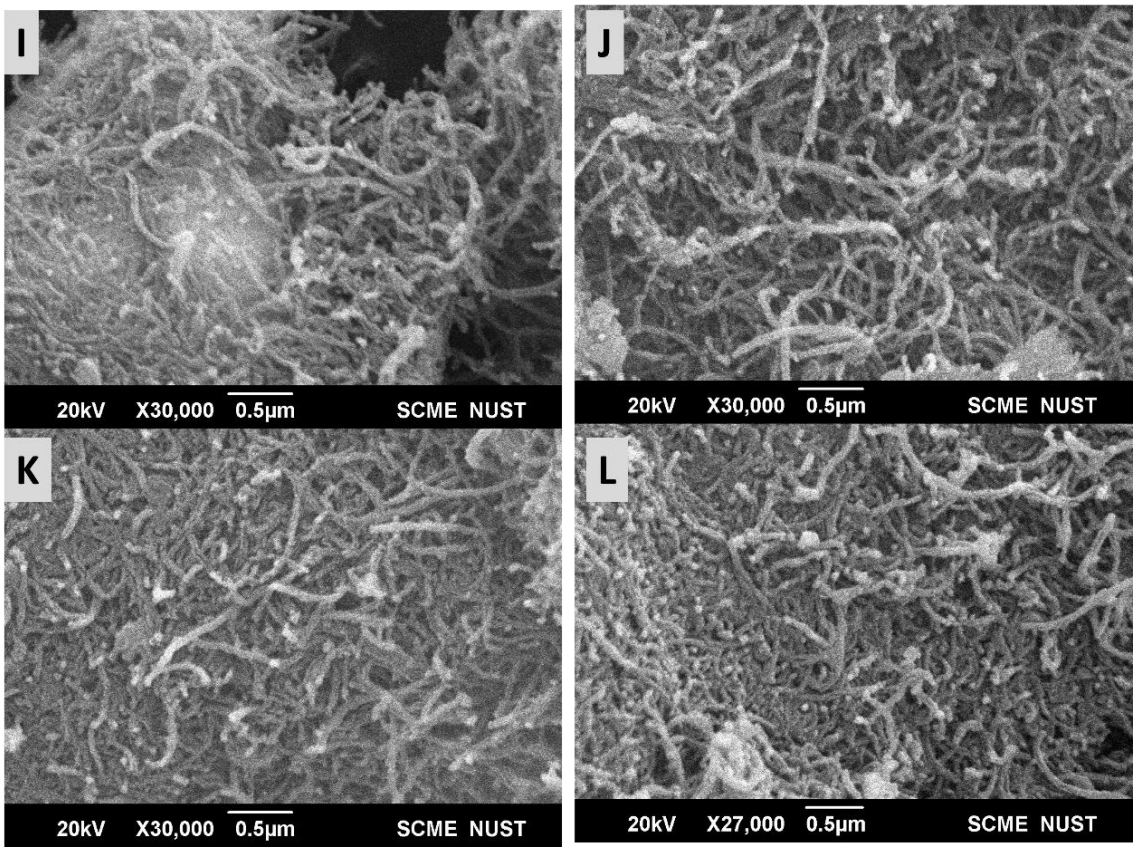

Figure 20: SEM results for $MoSe_2$/MWCNTs hybrids (1:1 - 1:4)

5.5. Electrochemical testing

5.5.1 Cyclic Voltammetry

The electrochemical analysis of all the modified nickel electrodes was performed in 3 M potassium hydroxide (KOH) electrolytic solution. The electrochemical measurements were carried out at a scan rate of 100 mV/s in potential range from 0 to 0.6 V.

Figure shows CVs of 5,10,15,20 MoSe2/MWCNTs, PANI, MWCNTs, MoSe2 and PANI MoSe2/MWCNTs. The values of oxidation peak currents for 5,10,15,20 MoSe2/MWCNTs, PANI, MWCNTs, MoSe2 and PANI MoSe2/MWCNTs composite were observed to be 7.6mA, 8.5mA, 9.2mA, 10.3mA, 11.5mA, 19.5mA, 24.8mA and 31.2mA at a potential of 0.394, 0.390, 0.385, 0.370, 0.364, 0.383, 0.379 and 0.347 V respectively. These peak current values demonstrate that the PANI

MoSe2/MWCNTs modified electrode exhibits a significantly higher peak current as compared to 5 MoSe2/MWCNTs. Possibly this rise in oxidation peak current is because of the electronic conductive nature of PANI which increases the active sites by providing a pathway for ion passage and electron transport for the redox process. Compared with each other 5,10,15 and 20 MoSe2/MWCNTs composites showed increase in the peak current which implies that the electron transfer reaction is intensified by the incorporation of MoSe2 nanoparticles likely because of the smaller size and larger surface area of nanoparticles. Notably, the current density of redox peak on PANI MoSe2/MWCNTs is higher than that of 5 MoSe2/MWCNTs. PANI, MWCNTs and MoSe2 individually showed increased current values as well which can be attributed to the conductive nature of all three. The synergistic effect caused by all the conductive nanomaterials enhances the charge flow.

Cyclic voltammetry was performed in the voltage range of 0 to 0.5V at various scan rates (10, 20, 30, 50, 80, and 100 mV/s) to investigate the charge storage behavior of the samples. The results are presented in Figure 9, providing insights into the electrochemical performance of the different samples. According to the equation provided and depicted in Figure 31, the specific capacitance (Cs) of the samples was determined using their cyclic voltammetry (CV) curves. The formula used for this calculation is as follows:

$$Cs = \frac{I(V)dV}{Av(V_2 - V_1)}$$

Here, (V2 - V1) represents the potential window, v is the scan rate in V/s (volts per second), and A is the working electrode area in cm². Table 4 presents a comparison of the calculated areal capacitance values for all samples at different scan rates, ranging from 5 mV/s to 100 mV/s. For instance, MoSe2 exhibits a capacitance of 1227.6F/g at a scan rate of 20 mV/s. In contrast, the capacitance values for MoSe2/MWCNTS samples MM (1:1 - 1:4) have the values of 436.71, 565.8, 640.90, 774.67 F/g respectively at the same scan rate. The specific capacitance of MWCNTs proves to be 1698.48F/g along with PANI at 1145.45F/g. However, the composite PANI-MWCNTs/MoSe2 shows a higher specific capacitance of 2748.48F/g.

Additionally, Table 4 demonstrates that as scan rates increase, the capacitance values decrease. This phenomenon is attributed to the limited diffusion of charge carriers at higher scan rates, a well-known effect. Nonetheless, the increasing current response as the scan rate rises implies excellent kinetics and reversibility of the electrode. Figure further illustrates that even at a high scan rate of

100 mV/s, the redox peaks remain discernible, affirming the material's exceptional high-rate capacity. Figure 22 shows the IPC and IPA graphs. Both the anodic peaks (Ipa) and the cathodic peaks (Ipc) increases linearly in the positive direction and negative direction, respectively. It may be because of the enhanced electrical polarization arising from the procedure of oxidation–reduction phenomenon. According to Figure both the anodic and cathodic peak currents are proportional to the square root of scan rates, suggesting a typical diffusion controlled electrochemical process.

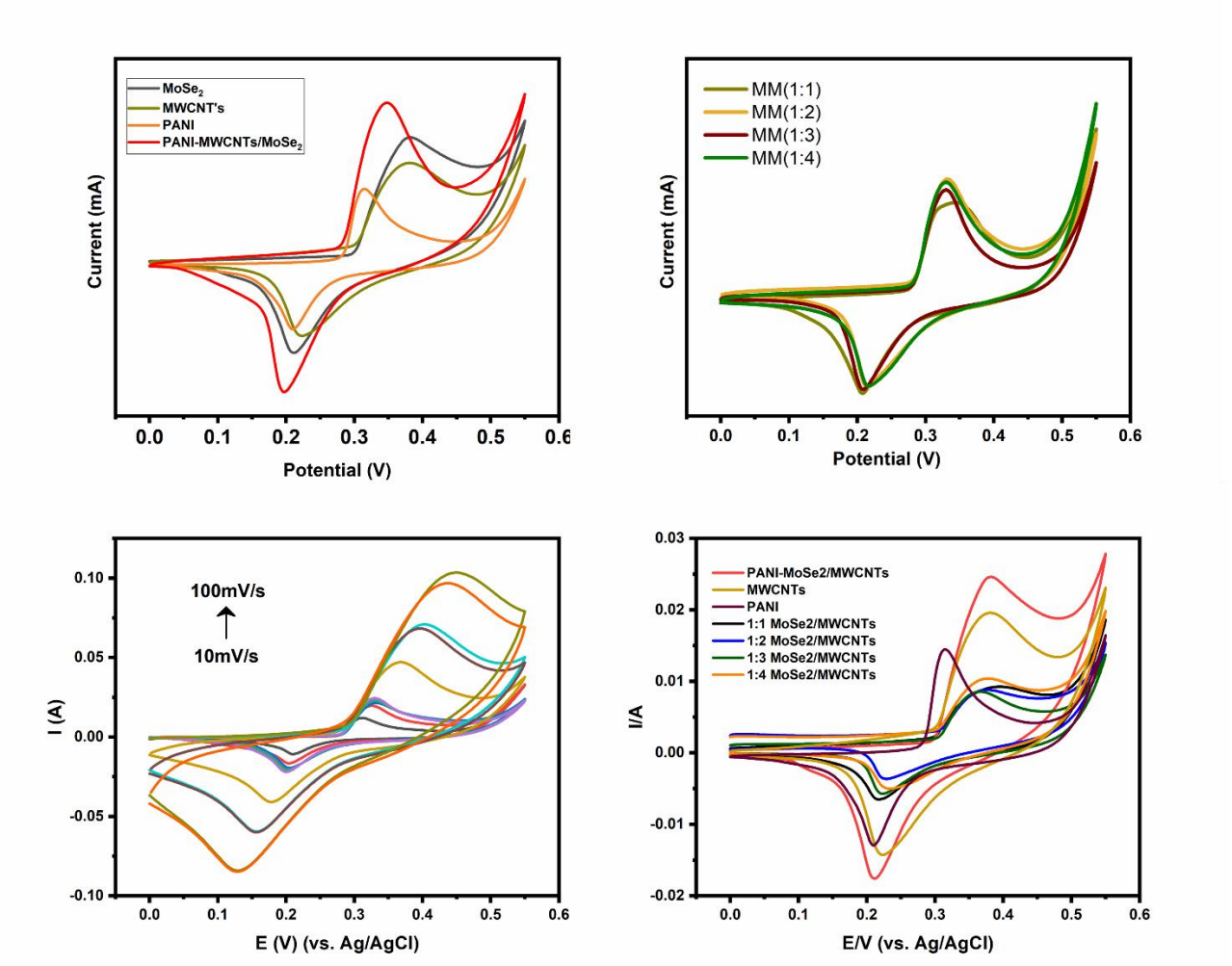

Figure 21: CV plot for (a) MoSe2, PANI, MWCNTS/MoSe2/PANI, MWCNTS (b)MoSe2/MWCNTs hybrid composites (1:1- 1:4) (c) PANI-MWCNTs/MoSe2 at scan rates of 5,20,40,60,80,100 mV/s

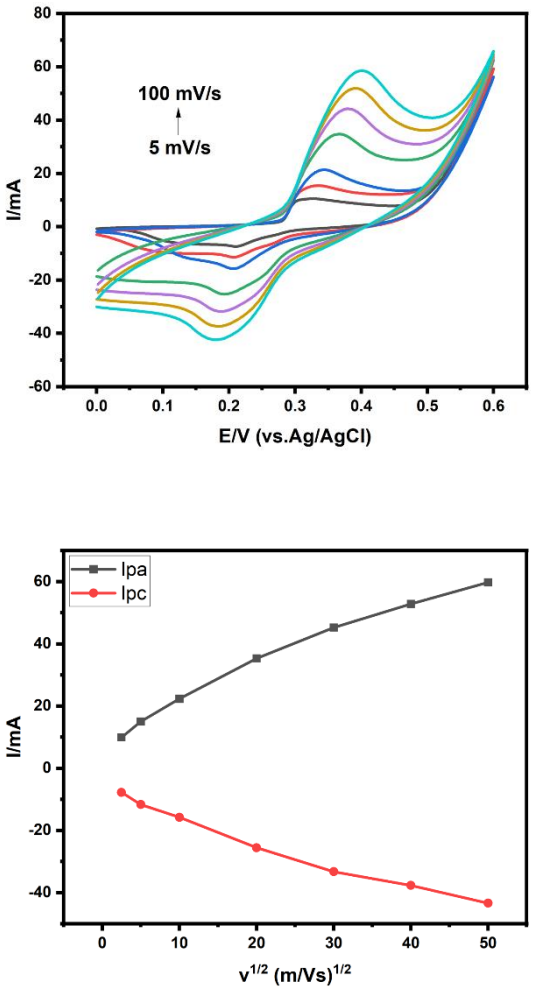

Figure 22 IPC &IPA Graphs

5.5.2. EIS

EIS (Electrochemical Impedance Spectroscopy) measurements were conducted on nickel foams in comparison to the base sample to understand their kinetic properties. Figure 9 (a) displays the Nyquist plot for all samples, ranging from low to high-frequency regions. The inset of figure 9 (b) shows the plot for mid- to high-frequency regions. Notably, each plot exhibits a linear part in both high- and low-frequency regions. The absence of a semicircular region in the high-frequency area indicates that all samples have minimal charge transfer resistance (Rct). Additionally, the high-frequency intercept on the real axis (Z') represents the series resistance (Rs), which includes contact resistance at the solid-liquid interface, internal resistance of the active material, and the electrolyte (ionic) resistance.

Electrochemical Impedance Spectroscopy was utilized to find out the electrode's kinetic performance. Nyquist plots of all the samples are shown in the figure below. EIS was done at 12 mV amplitude and the frequency changed between 100kHz – 0.1Hz. For all the plots there is a high and low frequency region. In the high-frequency region, the intercept at the real axis shows the solution resistance (Rs) while the straight lines in high-frequency region represent the resistance offered by the interface between the electrode, electrolyte, and the charges that transfer.

The Rs values in decreasing order for 5,10,15,20 MoSe2/MWCNTs, PANI, MWCNTs, MoSe2 and PANI MoSe2/MWCNTs composites were 1.908 Ω, 1.180 Ω, 1.178 Ω, 1.054 Ω, 1.004 Ω, 987.9 mΩ, 945.8 mΩ, and 913.9 mΩ respectively. This decrease in resistance indicates the composite PANI MoSe2/MWCNTs had negligible charge transfer at the interface between the electrode/electrolyte and greater electrical conductivity which is in coordination with the peak values studies through cyclic voltammetry curves. This performance indicates that the conductive polymer matrix in which MoSe2/MWCNTs were embedded provided the shortest diffusion path and access toward the electrolyte ions which resulted in decreased resistance and excellent current flow.

The absence of a semi-circle and therefore R_{ct} in the low-frequency regions displays straight lines indicating the impedance due to diffusion representing the movement of ions that occurred rapidly at the electrode's surface.

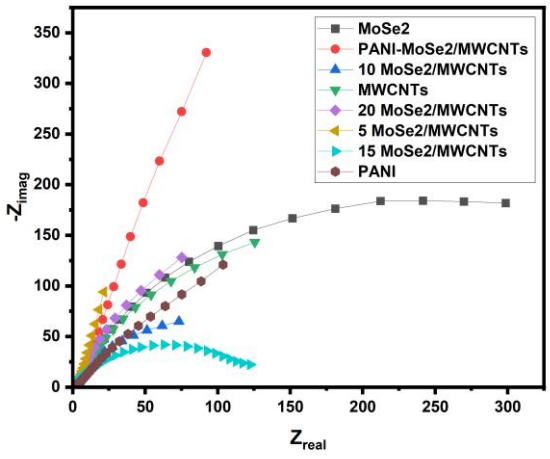

Liu, Y., Ren, L., Zhang, Z., Qi, X., Li, H., & Zhong, J. (2016). 3D binder-free MoSe2 nanosheets/carbon cloth electrodes for efficient and stable hydrogen evolution prepared by simple electrophoresis deposition strategy. *Scientific reports*, *6*(1), 22516.

5.6. Cyclic Charge – Discharge

Galvanostatic charge-discharge analysis was conducted to evaluate the charge-discharge characteristics, rate capability, and capacitance of PANI-$MoSe_2$/MWCNTs sample. Figure 22 illustrates the galvanostatic charge-discharge (GCD) curves for sample, within the same potential range of -1 to +1 volts. These GCD measurements were carried out using the same three-electrode electrochemical setup employed in cyclic voltammetry (CV) measurements, at various current densities of 0.5, 0.7, 1, 2, 5 A/g. Specific capacitances (Cs) of the samples were determined from the GCD curves using the following equation.

$$C_s = \frac{I(A) \times \Delta t(s)}{m(g) \times \Delta v(V)}$$

Hence, in the equation, I (in Amperes) represents the discharge current, Δt (in seconds) stands for the discharge duration, ΔV (in Volts) signifies the potential change resulting from the discharge, and m denotes the active mass of the material. The composite material shows the specific capacitance of 441 F/g. As the current density increases, there is a corresponding decrease in capacitance. This decrease can primarily be attributed to the reduced utilization rate of the active ingredient at higher current densities, as indicated by reference. The potential-time curves exhibit a relatively symmetrical pattern. In the cyclic voltammetry (CV) curves, the redox peaks align with the distinct potential plateaus observed at 0.0V for each curve, as shown in Figure 23 . Furthermore, deviations from linear behavior in the galvanostatic charge-discharge (GCD) profiles of all the electrodes suggest that the charge storage mechanisms involve a combination of faradic pseudocapacitive reactions and charge adsorption on the sample surface. n supercapacitor applications, achieving a prolonged cycling life with exceptional capacity retention is crucial for enhanced electrochemical performance. The capacity retention data for the PANI-$MoSe_2$/MWCNTs, subjected to nearly 300 cycles at a current density of 1 mA cm^{-2} (equivalent to 1000 μA/cm^2), is presented here. Impressively, even after 300 cycles, the sample maintains 90% of its initial capacitance value, underscoring its remarkable stability. This remarkable stability can be attributed to the high structural stability of High-Entropy Alloys (HEA), which prevents electrode expansion and contraction. Furthermore, the electrode exhibits a Coulombic efficiency of 96.35%, highlighting its efficiency in charge-discharge processes. Specific capacitance depends on the surface area of the electrode material and the adsorption of the ions in the electrolyte.

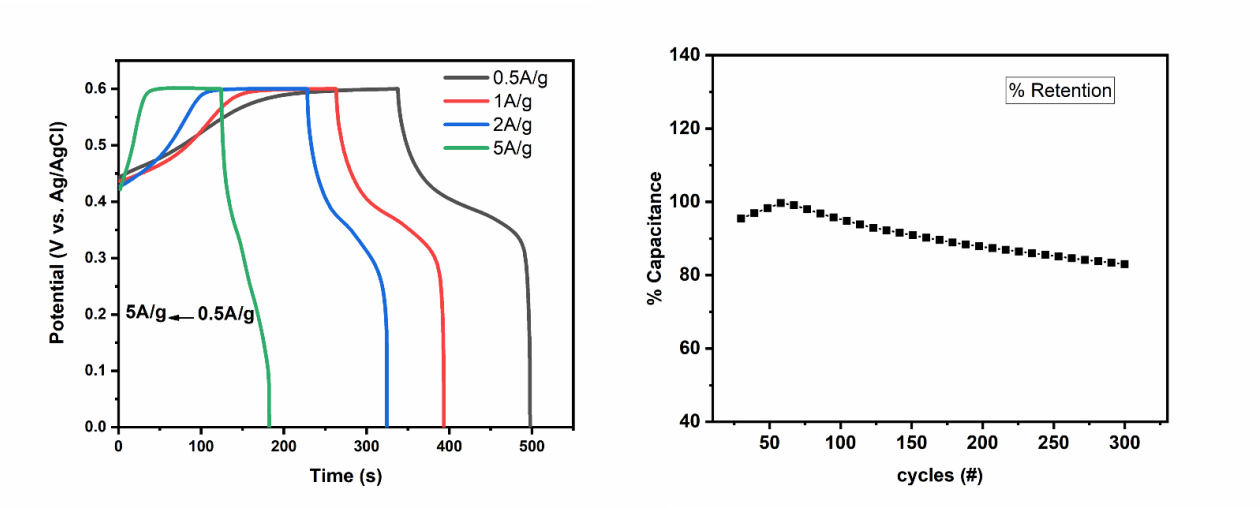

Figure 23 Charge-Discharge curve for PANI-$MoSe_2$/MWCNTs and Cyclic stability of sample at 0.5A/g current density

Conclusion

In this comprehensive study, we have delved into the potential of the PANI-MWCNTs/$MoSe_2$ composite electrode for supercapacitor applications, achieving an impressive specific capacitance. Our research journey has unearthed critical insights and implications that contribute significantly to the realm of energy storage devices. To begin with, the successful synthesis and thorough characterization of the PANI-MWCNTs/$MoSe_2$ electrode underscore the pivotal role of composite materials in elevating supercapacitor performance. The inclusion of $MoSe_2$ within the composite not only enhances the electrode's electrical conductivity but also augments its charge storage capacity. Our comprehensive electrochemical investigations have showcased the remarkable specific capacitance of 441 F/g, firmly establishing the PANI-MWCNTs/$MoSe_2$ electrode as an exceptionally efficient energy storage solution. Moreover, the observed intermolecular interactions between $MoSe_2$ nanoparticles and PANI offer intriguing insights into the enhanced electrochemical behavior of the composite, paving the way for potential optimizations in future research endeavors.

In summary, this thesis has illuminated the tremendous potential of the PANI-MWCNTs/$MoSe_2$ composite electrode for supercapacitor applications. These findings herald a new era in advanced energy storage devices, offering superior performance characteristics that hold great promise for a more sustainable and efficient future in energy storage technology. As we move forward, further exploration and refinement of this innovative composite material will undoubtedly contribute to the advancement of energy storage solutions.

References

1. Patel, A.B., et al., *Synergistic 2D MoSe (2) @WSe (2) nanohybrid heterostructure toward superior hydrogen evolution and flexible supercapacitor.* Nanoscale, 2022. **14**(17): p. 6636-6647.
2. Lei, W., et al., *An Overview of Bacterial Cellulose in Flexible Electrochemical Energy Storage.* ChemSusChem, 2020.
3. Lin, J., et al., *In Situ Synthesis of Vertical Standing Nanosized NiO Encapsulated in Graphene as Electrodes for High-Performance Supercapacitors.* Adv Sci (Weinh), 2018. **5**(3): p. 1700687.
4. *Supercapacitor*. 2018, New York, NY: Springer Berlin Heidelberg. pages cm.
5. Khaja Hussain, S. and J.H. Bang, *Overview of the oxygen vacancy effect in bimetallic spinel and perovskite oxide electrode materials for high-performance supercapacitors.* Phys Chem Chem Phys, 2023. **25**(17): p. 11892-11907.
6. Upadhyay, K.K., et al., *Capacitance response in an aqueous electrolyte of Nb2O5 nanochannel layers anodically grown in pure molten o-H3PO4.* Electrochimica Acta, 2018. **281**: p. 725-737.
7. Khan, Z., et al., *VO (2) Nanostructures for Batteries and Supercapacitors: A Review.* Small, 2021. **17**(4): p. e2006651.
8. Kothandam, G., et al., *Recent Advances in Carbon-Based Electrodes for Energy Storage and Conversion.* Adv Sci (Weinh), 2023. **10**(18): p. e2301045.
9. Choi, K.M., et al., *Supercapacitors of nanocrystalline metal-organic frameworks.* ACS Nano, 2014. **8**(7): p. 7451-7.
10. Díez-Pascual, A.M. and A. Rahdar, *Graphene-Based Polymer Composites for Flexible Electronic Applications.* Micromachines (Basel), 2022. **13**(7).
11. Nguyen, T.K., S. Aberoumand, and D.V. Dao, *Advances in Si and SiC Materials for High-Performance Supercapacitors toward Integrated Energy Storage Systems.* Small, 2021. **17**(49): p. e2101775.
12. Zhao, X., B.M. Sánchez, P.J. Dobson, and P.S. Grant, *The role of nanomaterials in redox-based supercapacitors for next generation energy storage devices.* Nanoscale, 2011. **3**(3): p. 839-55.
13. Noori, A., et al., *Towards establishing standard performance metrics for batteries,*

supercapacitors and beyond. Chem Soc Rev, 2019. **48**(5): p. 1272-1341.

14. Oliveira, D.A., L.H.S. Gasparotto, and J.R. Siqueira, Jr., *Processing of nanomaterials in Layer-by-Layer films: Potential applications in (bio)sensing and energy storage.* An Acad Bras Cienc, 2019. **91**(2): p. e20181343.
15. Pan, S., et al., *Recognition of Ionic Liquids as High-Voltage Electrolytes for Supercapacitors.* Front Chem, 2020. **8**: p. 261.
16. Pervez, S. and M.Z. Iqbal, *Capacitive and Diffusive Contributions in Supercapacitors and Batteries: A Critique of b-Value and the nu-nu (1/2) Model.* Small, 2023: p. e2305059.
17. Aravinda, L.S., et al., *Fabrication and performance evaluation of hybrid supercapacitor electrodes based on carbon nanotubes and sputtered TiO2.* Nanotechnology, 2016. **27**(31): p. 314001.
18. Ariga, K., M. Matsumoto, T. Mori, and L.K. Shrestha, *Materials nanoarchitectonics at two-dimensional liquid interfaces.* Beilstein J Nanotechnol, 2019. **10**: p. 1559-1587.
19. Badwal, S.P., et al., *Emerging electrochemical energy conversion and storage technologies.* Front Chem, 2014. **2**: p. 79.

20. Balqis, N., et al., *An Overview of Recycling Wastes into Graphene Derivatives Using Microwave Synthesis; Trends and Prospects.* Materials (Basel), 2023. **16**(10).
21. Zong, W., et al., *Recent advances and perspectives of 3D printed micro- supercapacitors: from design to smart integrated devices.* Chem Commun (Camb), 2022. **58**(13): p. 2075-2095.
22. Bressi, A.C., A. Dallinger, Y. Steksova, and F. Greco, *Bioderived Laser-Induced Graphene for Sensors and Supercapacitors.* ACS Appl Mater Interfaces, 2023. **15**(30): p. 35788-35814.
23. Zhao, X., K. Tao, and L. Han, *Self-supported metal-organic framework-based nanostructures as binder-free electrodes for supercapacitors.* Nanoscale, 2022. **14**(6): p. 2155-2166.
24. Sung, J. and C. Shin, *Recent Studies on Supercapacitors with Next-Generation Structures.* Micromachines (Basel), 2020. **11**(12).
25. Zhou, G., et al., *Nanowires for Electrochemical Energy Storage.* Chem Rev, 2019. **119**(20): p. 11042-11109.

26. Zhao, J., X. Zou, P. Sun, and G. Cui, *Three-Dimensional Bi-Continuous Nanoporous Gold/Nickel Foam Supported MnO (2) for High Performance Supercapacitors.* Sci Rep, 2017. **7**(1): p. 17857.
27. Zhao, L., et al., *Laser Synthesis and Microfabrication of Micro/Nanostructured Materials Toward Energy Conversion and Storage.* Nanomicro Lett, 2021. **13**(1): p. 49.
28. Zhang, T., et al., *Synthesis of graphene and related two-dimensional materials for bioelectronics devices.* Biosens Bioelectron, 2017. **89**(Pt 1): p. 28-42.
29. Wang, T., et al., *MoS (2)-Based Nanocomposites for Electrochemical Energy Storage.* Adv Sci (Weinh), 2017. **4**(2): p. 1600289.
30. Wang, H., et al., *Three-dimensional graphene-based materials: Synthesis and applications from energy storage and conversion to electrochemical sensor and environmental remediation.* Adv Colloid Interface Sci, 2015. **221**: p. 41-59.
31. Timmerman, M.A., et al., *Metal Oxide Nanosheets as 2D Building Blocks for the Design of Novel Materials.* Chemistry, 2020. **26**(42): p. 9084-9098.
32. Allahbakhsh, A. and A.R. Bahramian, *Self-assembled and pyrolyzed carbon aerogels: an overview of their preparation mechanisms, properties, and applications.* Nanoscale, 2015. **7**(34): p. 14139-58.
33. Abdalla, A.M., et al., *Nickel oxide nanotube synthesis using multiwalled carbon nanotubes as sacrificial templates for supercapacitor application.* Nanotechnology, 2017. **28**(7): p. 075603.
34. Wang, B., C. Hu, and L. Dai, *Functionalized carbon nanotubes and graphene-based materials for energy storage.* Chem Commun (Camb), 2016. **52**(100): p. 14350-14360.
35. Akib Hasan, M., S. Sayantha Aniv, and M. Mominul Islam, *Carbon Nanosheets-Based Supercapacitor Materials: Recent Advances and Prospects.* Chem Rec, 2023: p. e202300153.
36. Vinoth, V., et al., *SnO2-decorated multiwalled carbon nanotubes and Vulcan carbon through a sonochemical approach for supercapacitor applications.* Ultrason Sonochem, 2016. **29**: p. 205-12.
37. Tang, Q., et al., *Quasi 2D Mesoporous Carbon Microbelts Derived from Fullerene Crystals as an Electrode Material for Electrochemical Supercapacitors.* ACS Appl Mater Interfaces, 2017. **9**(51): p. 44458-44465.

38. Sun, Y., et al., *Surface chemistry and structure manipulation of graphene-related materials to address the challenges of electrochemical energy storage.* Chem Commun (Camb), 2023. **59**(18): p. 2571-2583.

39. Shi, J., et al., *Smart Textile-Integrated Microelectronic Systems for Wearable Applications.* Adv Mater, 2020. **32**(5): p. e1901958.

40. Zhu, Y., et al., *High-Voltage MXene-Based Supercapacitors: Present Status and Future Perspectives.* Small Methods, 2023: p. e2201609.

41. Zhang, J., et al., *MXene: a potential candidate for yarn supercapacitors.* Nanoscale, 2017. **9**(47): p. 18604-18608.

42. Zhang, F., et al., *Organic/Inorganic Hybrid Fibers: Controllable Architectures for Electrochemical Energy Applications.* Adv Sci (Weinh), 2021. **8**(22): p. e2102859.

43. Zhang, C., L. Zhang, and G. Yu, *Eutectic Electrolytes as a Promising Platform for Next-Generation Electrochemical Energy Storage.* Acc Chem Res, 2020. **53**(8): p. 1648- 1659.

44. Zhang, Z., et al., *Single-Walled Carbon Nanohorns for Energy Applications.* Nanomaterials (Basel), 2015. **5**(4): p. 1732-1755.

45. Ansari, S.N., M. Saraf, Z. Abbas, and S.M. Mobin, *Heterostructures of MXenes and transition metal oxides for supercapacitors: an overview.* Nanoscale, 2023.

46. *Materials development for active/passive components of a supercapacitor*. 2018, New York, NY: Springer Berlin Heidelberg. pages cm.

47. Basha, S.I., et al., *Construction Building Materials as Potential for Structural Supercapacitor Applications.* Chem Rec, 2022. **22**(11): p. e202200134.

48. Chanut, N., et al., *Carbon-cement supercapacitors as a scalable bulk energy storage solution.* Proc Natl Acad Sci U S A, 2023. **120**(32): p. e2304318120.

49. Britton, M.M., *MRI of chemical reactions and processes.* Prog Nucl Magn Reson Spectrosc, 2017. **101**: p. 51-70.

50. Chatterjee, A., et al., *Exploring the Charge Storage Dynamics in Donor-Acceptor Covalent Organic Frameworks Based Supercapacitors by Employing Ionic Liquid Electrolyte.* Small, 2023: p. e2303189.

51. Gong, F., et al., *Hierarchical Mn(2)O(3) Microspheres In-Situ Coated with Carbon for Supercapacitors with Highly Enhanced Performances.* Nanomaterials (Basel), 2017. **7**(12).

52. Akib Hasan, M., S. Sayantha Aniv, and M. Mominul Islam, *Carbon Nanosheets-Based Supercapacitor Materials: Recent*